Ore Geology Reviews 77 (2016) 97–116

Contents lists available at ScienceDirect

Ore Geology Reviews

journal homepage: www.elsevier.com/locate/oregeorev

Partitioning of trace elements in co-crystallized sphalerite–galena–chalcopyrite hydrothermal ores

Luke L. George [a,*], Nigel J. Cook [b], Cristiana L. Ciobanu [b]

[a] School of Physical Sciences, University of Adelaide, Adelaide, SA 5005, Australia
[b] School of Chemical Engineering, University of Adelaide, Adelaide, SA 5005, Australia

ARTICLE INFO

Article history:
Received 12 November 2015
Received in revised form 12 February 2016
Accepted 16 February 2016
Available online 18 February 2016

Keywords:
Trace element
Sphalerite
Galena
Chalcopyrite
Partitioning
Laser-ablation inductively-coupled plasma mass spectrometry

ABSTRACT

There is an abundance of published trace element data for sphalerite, galena and chalcopyrite in natural systems, yet for a co-crystallized assemblage comprising these base metal sulphides, there is no detailed understanding of the preferred host of many trace elements. Laser-ablation inductively-coupled plasma mass spectrometry trace element maps and spot analyses were generated on 17 assemblages containing co-crystallized sphalerite and/or galena and/or chalcopyrite from 9 different ore deposits. These deposits are representative of different ore types, geologic environments and physiochemical conditions of ore formation, as well as superimposed syn-metamorphic remobilisation and recrystallization. The primary factors that control the preferred base metal sulphide host of Mn, Fe, Co, Cu, Zn, Ga, As, Se, Ag, Cd, In, Sb, Te, Tl and Bi are element oxidation state, ionic radius of the substituting element, element availability and the maximum trace element budget that a given sulphide mineral can accommodate. Temperature, pressure, redox conditions at time of crystallization and metal source, do not generally appear to influence the preferred base metal sulphide host of all the trace elements. Exceptions are Ga, In and Sn recrystallized at high metamorphic grades, when the preferred host of Ga and Sn usually becomes chalcopyrite. In more typical lower temperature ores, the preferred host of Ga is sphalerite. Indium concentrations also increase in chalcopyrite during recrystallization. At lower temperatures the partitioning behaviour of Sn remains poorly constrained and shows little predictable pattern among the data here. The results obtained may be used as a tool to assess co-crystallization. If trace element distributions in a given base metal sulphide assemblage match those reported here, and assuming those distributions have not been significantly altered post (re-) crystallization, then it may be suggestive of a co-crystallized assemblage. Such information provides a foundation for novel attempts to develop trace element-in-sulphide geothermometers.

1. Introduction

Application of multi-element microanalytical techniques, e.g., micro-particle-induced X-ray emission (μ-PIXE), secondary ion mass spectrometry (SIMS), electron probe microanalysis (EPMA), or laser-ablation inductively-coupled plasma mass spectrometry (LA-ICP-MS), has become commonplace in many fields of geology, including studies relating to ore genesis. This is largely due to the accurate *in-situ* concentration data these techniques can generate, with both sub-part-per-million level precision (for μ-PIXE, SIMS and LA-ICP-MS) and micrometre-scale spatial resolution. As a result, large amounts of trace element data have been published on many common ore minerals, including the base metal sulphides (BMS), sphalerite (ZnS), galena (PbS) and chalcopyrite ($CuFeS_2$) (e.g., McIntyre et al., 1984; Cabri et al., 1985; Foord and Shawe, 1989; Cabri, 1992; Huston et al., 1995; Larocque et al., 1995; Moggi-Cecchi et al., 2002; Cook et al., 2009, 2011a; Lockington et al., 2014; George et al., 2015). As such, the diversity of trace elements and ranges of concentration that these sulphides can incorporate has been relatively well documented. However, the partitioning of trace elements between co-crystallized BMS in hydrothermal ores is not well constrained. This is in contrast to the generally well understood partitioning behaviour of trace elements, including the platinum group elements and gold, between pyrrhotite, pentlandite, pyrite and BMS in magmatic sulphide ore deposits (e.g., Holwell and McDonald, 2010; Dare et al., 2011, and references therein).

Previous work that addresses trace element concentrations within individual sulphides has demonstrated the need to understand trace element partitioning patterns in hydrothermal BMS assemblages. This study aims to identify whether trace element partitioning between co-crystallized sphalerite, galena and chalcopyrite is predictable, and if so, to determine the primary controls on this partitioning. Such information can underpin tools for assessing whether a given BMS assemblage co-crystallized, and also potentially to enable constraints to be placed on conditions of BMS co-crystallization. In this contribution, we acknowledge the role that temperature, pressure, redox conditions at

* Corresponding author.
E-mail address: luke.george@adelaide.edu.au (L.L. George).

http://dx.doi.org/10.1016/j.oregeorev.2016.02.009
0169-1368/

time of crystallization and metal source have on partitioning trends, but will emphasize the important role played by trace element oxidation state and, closely related to that, ionic radius.

2. Background

George et al. (2015) presented a reconnaissance study of trace elements in galena and showed that a range of elements are systematically hosted in solid solution within galena from SEDEX, epithermal, skarn, VMS, orogenic Au and porphyry BMS ores. A number of these elements show predictable behaviours when preferentially partitioning into galena together with other elements via coupled substitution (e.g., Bi and Sb with Ag, Tl and Cu), as well as systematic partitioning between two coexisting minerals (e.g., Tl between galena and sphalerite). It was, however, also noted that the presence or absence of other co-existing sulphides can influence the distributions of some trace elements within some deposit types (e.g., Sn distribution patterns in galena from recrystallized massive sulphide deposits containing chalcopyrite). It is thus difficult to make broad conclusions about the partitioning behaviour of trace elements when galena is largely considered in isolation. In order to gain a more accurate understanding of the partitioning behaviour of trace elements between two or more co-crystallizing BMS in a given ore system, the chemistry of any sulphide phase needs to be considered in the context of the complete BMS assemblage. In light of this, the present study sets out to answer the following question: do trace elements exhibit predictable partitioning behaviours among sphalerite, galena and chalcopyrite when the three minerals co-crystallize?

One of the outcomes of contemporary *in-situ* microanalytical investigation of sulphides is the recognition that many sulphides previously considered homogenous at the grain-scale, are in fact not always so (e.g., molybdenite; Ciobanu et al., 2013). Thus some published trace element datasets, especially those obtained before the 1980s, may simply represent averages of multiple, compositionally-distinct zones within a single grain. Recognition of elements present in solid solution, or occurring in micro-inclusions of distinct mineral phases, has been traditionally gained by carefully assessing all element concentrations and seeking combinations of elements that suggest inclusions [e.g., proton microprobe work of Cabri et al. (1985) or Huston et al. (1995)]. The LA-ICP-MS technique, however, may provide indirect evidence for the presence of micro-inclusions. If these are large enough and heterogeneously distributed, they will be recognized on time-resolved down-hole ablation profiles (e.g., George et al., 2015). The ability to distinguish a trace element in solid solution from one occurring as nano- to microscale inclusions of a distinct mineral phase is critical for interpretation of such data since it is likely that only those trace elements that are substituted into the crystal lattice of a sulphide would reveal systematic partitioning patterns. The LA-ICP-MS mapping technique allows for a visual comparison of multiple compositionally-distinct zones within a single grain or co-existing assemblage. Assuming such zoning occurs at a scale larger than the spatial resolution, even trace element heterogeneity may be recognized. LA-ICP-MS also offers advantages over SIMS in that the technique is more flexible with standards, significantly cheaper to run, and perhaps most importantly, offers simultaneous analysis of >25 elements.

Despite some of the limitations of modern microanalysis discussed, a review of the published literature provides a background to the data reported here. Table 1 summarizes the range of trace elements measured within sphalerite, galena and chalcopyrite and their typical concentrations as determined from analysis of natural specimens. The table also lists the experimentally-determined solubility limits of several of these elements.

3. Sample suite

The study covered 17 BMS-bearing samples from nine different skarn, epithermal and SEDEX deposits in Australia, Norway and Romania (Table 2 and references therein). Selected samples contain coexisting sphalerite and/or galena and/or chalcopyrite, which textural evidence suggests co-crystallized at equilibrium. SEDEX deposits metamorphosed at greenschist facies (Fig. 1A) retain primary syn-sedimentary textures while epithermal (Fig. 1B) and skarn (Fig. 1C) systems commonly display 120° triple junctions between sulphide grains. Such grain boundaries are similar to those in SEDEX deposits metamorphosed at amphibolite facies and above (Fig. 1D, E) which display a coarser grain size and characteristic 120° triple junctions developed during equilibrium recrystallization. Though the sample suite is not representative of entire mineral associations in each different deposit, the samples were selected because they represent the same co-crystallized BMS assemblage formed at different physiochemical conditions in different ore types. They are thus representative for the purposes relevant to this study.

Skarn ores are represented by 5 samples from Baita Bihor and Oravita, two deposits located ~350 km apart along the Late Cretaceous Banatitic Magmatic and Metallogenetic Belt, Romania (BMMB; e.g., Ciobanu et al., 2002). The BMMB contains a range of magmatic-hydrothermal mineralization styles relating to the same magmatic event, and formed in subduction settings during Neotethys closure. The belt is well known for exotic trace mineral signatures including a most prominent Bi-mineral signature (e.g., Ciobanu et al., 2002). The Cu–Mo–Pb–Zn skarn deposit at Baita Bihor boasts the most complex geochemical signature [Bi–Ag–W–Se–Te–Ni–Co–Sn] among the deposits considered here. Consequently, this skarn exhibits a diverse sulphide mineralogy, including As-, Sb-, and Bi-sulphosalts and Bi- and Ag-tellurides (Cioflica et al., 1995, 1997; Cook and Ciobanu, 2003; Ilinca et al., 2012; Ciobanu et al., 2014). The Antoniu orepipe is Cu-dominant and proximal to the granitoid-derived source fluids. It contains Pb–Zn ores near the marble/skarn contact and lesser amounts within the Cu zone. The distinctly Pb–Zn Marta orepipe is a distal zone, ~1.2 km ENE from Antoniu.

Oravita is one of the many Cu–Au skarns that are satellite to porphyry Cu–Mo-intrusions within the Banat region (SW Romania and Serbia), known for its rich deposits (e.g., von Cotta, 1864). As with many Cu skarns, it also contains base metal ores and minor W-mineralization (Gheorghitescu, 1975; Cioflica and Vlad, 1981; Constantinescu et al., 1988). Oravita is one of the few localities where gehlenite skarns are known along the BMMB (Katona et al., 2003; Marincea et al., 2011). Although such skarns are barren, they provide an upper temperature limit (~750 °C) for initiation of the skarn system close to intrusion contacts.

Four samples come from Herja and Toroiaga, Baia Mare District, Romania. Both deposits are polymetallic epithermal vein systems of Neogene age with a diverse mineralogy, including well-known occurrences of Pb–Ag–Sb–As or -Bi sulphosalts. Cu–Au–Pb–Zn veins at Toroiaga are located 90 km to the east of the Pb–Zn–Ag veins at Herja, but related to the same regional-scale E–W-trending Dragos Voda fault (Neubauer et al., 2005 and references therein). Toroiaga is somewhat distinct from other deposits in the Baia Mare District in that its veins are thought to have formed at higher temperatures (as much as 400 °C; Cook, 1997), i.e., unlike the typical Pb–Zn–Ag veins common in Baia Mare.

Eight samples have been selected from five SEDEX deposits (Table 2). These are divided into two groups based on metamorphic grade. Only those deposits metamorphosed at conditions above greenschist facies show clear textural evidence for recrystallization of the BMS assemblage (e.g., coarse annealed textures, commonly with 120° triple junctions between grains; Fig. 1D, E). Recrystallization allows for pervasive re-partitioning of trace elements from the primary low-temperature SEDEX distributions to the distributions preferred at high metamorphic temperatures and pressures, followed by slow cooling. Recrystallized SEDEX deposits (5 samples) can thus be distinguished from those of lower metamorphic grades (3 samples).

Those SEDEX deposits of lower metamorphic grade include Kapp Mineral and Mt. Isa. Kapp Mineral is a minor occurrence from the Hecla Hoek Complex, Svalbard Archipelago, Norway. Mineralization is of an undetermined, possibly late Precambrian age but has clearly

Table 1
Review of relevant literature relating to trace elements in sphalerite, galena and chalcopyrite.

	Sphalerite			Galena			Chalcopyrite		
Specific references	Cook et al. (2009); Johan (1988); Lockington et al. (2014); Ye et al. (2011)			Blackburn and Schwendeman (1977); Foord and Shawe (1989); George et al. (2015)			Bajwah et al. (1987); Harris et al. (1984); Moggi-Cecchi et al. (2002)		
General references	Bethke and Barton (1971); Emslie and Beukes (1981); McIntyre et al. (1984); Cabri et al. (1985); Qian (1987); Brill (1989); Cabri (1992); Huston et al. (1995)								
Trace element	Present in solid solution	Typical concentration (ppm)	Solubility limit	Present in solid solution	Typical concentration (ppm)	Solubility limit	Present in solid solution	Typical concentration (ppm)	Solubility limit
Mn	Common	Hundreds–thousands (rarely wt.%)	7 mol.% MnS at 600 °C Bethke and Barton (1971)	Uncommon	–	3.5 mol.% MnS at 850 °C Bethke and Barton (1971)	Uncommon	Few	–
Fe	Common	Thousands–wt.%	52 mol.% FeS at 700 °C Lepetit et al. (2003)	Uncommon	–	–	–	–	–
Co	Occasional	Tens–hundreds	41 mol.% CoS at 1000 °C Becker and Lutz (1978)	No/questionable	–	–	Occasional	Tens–hundreds	–
Cu	Occasional	Tens–hundreds	10.7 mol.% CuS at 800 °C Kojima and Sugaki (1984)	Uncommon	Few–tens	Extremely low below 200 °C Craig and Kullerud (1968)	–	–	–
Zn	–	–	–	Uncommon	–	–	Occasional	Tens–hundreds	0.9 at.% Zn at 500 °C Kojima and Sugaki (1985)
Ga	Occasional	Tens–hundreds	20 mol.% Ga_2S_3 below 800 °C Krämer et al. (1987)	No/questionable	–	–	No/questionable	–	–
Ge	Occasional	Tens–hundreds	–	Uncommon	–	–	Occasional	Tens–hundreds	–
As	Uncommon	–	–	Uncommon	–	–	Uncommon	Few–tens	–
Se	Occasional	Tens–hundreds	2.7 mol.% ZnSe at 600 °C Bethke and Barton (1971)	Common	Hundreds	Complete ss with PbSe below 1050 °C Liu and Chang (1994)	Occasional	Tens–hundreds	0.5 mol.% $Cu_{.526}Fe_{.526}Se$ at 390 °C Bethke and Barton (1971)
Ag	Occasional	Tens	–	Common	Hundreds–thousands	Complete ss with $Ag(Sb,Bi)Pb_2$ above 420 °C Chutas et al. (2008)	Common	Tens–hundreds	–
Cd	Common	Hundreds–thousands (rarely wt.%)	6 mol.% CdS at 600 °C Chen et al. (1988)	Occasional	Few–hundreds	–	Uncommon	Few	–
In	Common	Tens–hundreds (rarely thousands)	~80 mol.% $CuInS_2$ below 1000 °C Sombuthawee et al. (1978)	Uncommon	–	–	Occasional	Tens–hundreds	–
Sn	Occasional	Tens–hundreds (rarely thousands)	–	Occasional	Few–tens	–	Occasional	Few–tens	–
Sb	Uncommon	–	–	Common	Hundreds	Complete ss with $Ag(Sb,Bi)Pb_2$ above 420 °C Chutas et al. (2008)	Uncommon	–	–
Te	Uncommon	Few	–	Occasional	Few–hundreds	10 mol.% PbTe at 700 °C Liu and Chang (1994)	Uncommon	Few	–
Hg	Occasional	Tens	–	Uncommon	–	–	No/questionable	–	–
Tl	Occasional	Few–tens	–	Common	Few–tens	–	No/questionable	–	–
Bi	No/Questionable	–	–	Common	Hundreds–thousands	Complete ss with $Ag(Sb,Bi)Pb_2$ above 420 °C Chutas et al. (2008)	Uncommon	Few	–

been reworked such that it now aligns with Tertiary faults at the contact between Late Proterozoic and Palaeozoic sequences. Mt. Isa is, by contrast, a large Australian Proterozoic deposit located in the Mt. Isa Inlier, Queensland. The deposit has been metamorphosed to greenschist facies (Rubenach, 1992; Hannan et al., 1993; Large et al., 2005).

The recrystallized SEDEX deposits metamorphosed at amphibolite facies and above include Broken Hill, Bleikvassli and Mofjellet. Broken Hill is a giant Australian Proterozoic deposit located in the Curnamona Province, New South Wales (Plimer, 2007). It has experienced granulite facies metamorphism, and possible partial melting (Frost et al., 2005; Spry et al., 2008).

Bleikvassli and Mofjellet are located approximately 45 km apart in the Lower Palaeozoic Norwegian Caledonides. Mofjellet underwent amphibolite facies metamorphism whereas Bleikvassli experienced slightly higher upper amphibolite to lower granulite facies metamorphism. As a result of remobilization during regional metamorphic overprinting, the recrystallized SEDEX deposits exhibit a diverse mineralogy similar to some epithermal deposits (e.g., Cook et al., 1998).

4. Experimental methods

Each sample was prepared as a polished block of differing size. Sample characterization and selection of areas free of any noticeable inclusions for trace element analysis and element mapping was conducted using reflected light microscopy and backscattered electron (BSE) imaging.

Both LA-ICP-MS element mapping and spot analysis was carried out on a Resonetics M-50-LR 193 nm Excimer laser attached to an Agilent 7700cx Quadrupole ICP mass spectrometer (Adelaide Microscopy). The Resonetics laser uses a two-volume ablation cell designed by Laurin Technic Pty. for outstanding trace element sensitivity, washout and stability (Müller et al., 2009). Ablation takes place in an atmosphere of UHP He (0.7 L/min), creating an aerosol mixed with Ar (0.93 L/min) after leaving the ablation cell. The mix is then passed through a pulse-homogenizing device or "squid" before being directly introduced into the torch. Calibration of the ICP-MS is performed regularly in order to maximize the sensitivity on the isotopes of interest, whilst also keeping production of molecular oxide species (i.e., $^{232}Th^{16}O/^{232}Th$) and doubly charged ion species (i.e., $^{140}Ce^{2+}/^{140}Ce^{+}$) as low as possible, and usually <0.2%.

LA-ICP-MS element maps were made on selected areas to provide trace element concentrations as well as visualization of their distributions within individual sulphide grains. Mapping was performed by ablating sets of parallel line rasters in a grid across the sample. The laser spot size varied between 7–10 μm keeping the scan speed at a constant 10 μm/s. This ensured the desired sensitivity of elements of interest, as well as adequate spatial resolution depending on the size of the mapped area. The spacing between the lines was adjusted to match the laser spot size. A laser repetition of 10 Hz was selected at a constant energy output of 100 mJ. Thirty elements were analysed with the dwell time set to 0.01 s for all elements except for In, Au, and Tl which were set to 0.05 s, resulting in a total sweep time of 0.481 s. Thirty seconds of background was acquired by the ICP-MS before each raster was ablated, followed by a delay of 20 s for cell wash-out, gas stabilization, and computer processing time. At the beginning and end of each mapping run identical rasters were done on the MASS-1 (formerly PS-1) sulphide reference material (Wilson et al., 2002). Element maps were compiled and processed using the program Iolite, following the method described in George et al. (2015).

LA-ICP-MS spot analysis was carried out with the laser beam energy output set at 100 mJ at a 26 μm spot size while analysing sphalerite and chalcopyrite. When analysing galena, the energy output was set at 80 mJ and the spot size was set at 8 μm to ensure the ICP-MS was not oversaturated with Pb. A laser repetition rate of 10 Hz was used in all cases. Total acquisition time for each analysis was 60 s, comprising 30 s background measurement followed by 30 s of sample ablation. A 40 s delay was allowed after each spot analysis to ensure adequate cell wash-out, gas stabilization, and computer processing time. The following isotope suite was analysed: ^{34}S, ^{55}Mn, ^{57}Fe, ^{59}Co, ^{60}Ni, ^{65}Cu, ^{66}Zn, ^{69}Ga, ^{72}Ge, ^{75}As, ^{82}Se, ^{95}Mo, ^{107}Ag, ^{111}Cd, ^{115}In, ^{118}Sn, ^{121}Sb, ^{125}Te, ^{182}W, ^{197}Au, ^{202}Hg, ^{205}Tl, ^{207}Pb, and ^{209}Bi. Dwell times for each element were set to 0.01 s except for In, Au and Tl which were set to 0.05 s. Batches of up to 10 analyses were bracketed by repeat analyses of the MASS-1 standard. This allowed for the monitoring of, and correction for, instrumental drift by applying a linear correction based on the bracketed MASS-1 analyses. Data calculations were carried out using

Table 2
Summary of deposits and samples used in this study.

Deposit/type	Samples	Ore mineralogy	Conditions of formation or metamorphism	References
Herja, Romania Epithermal (*Neogene*)	Hj13	Gn–Cp–Py–Tet–Sp–Po–Ap–Ss–St	Formed at ~<200 °C Borcos et al. (1975)	Lang (1979) and Cook and Damian (1997)
Toroiaga, Romania Epithermal (*Neogene*)	TOR191 TOR197 Emeric2	Cp–Py–Sp–Gn Py–Sp–Cp–Gn–Ss Py–Cp–Gn–Sp	Formed at ~350 °C Cook (1997)	Szöke and Steclaci (1962) and Gotz et al. (1990)
Baita Bihor, Romania Skarn Antoniu orepipe — proximal Marta orepipe — distal (*Cretaceous*)	BBH16B (Antoniu) BBH20 (Antoniu) BB55 (Antoniu) BBH32 (Marta)	Gn–Sp–Cp Gn–Sp–Cp Gn–Sp–Cp Gn–Sp–Py	Formed at ~500 °C (proximal),~375 °C (distal)	Cioflica et al. (1971, 1977) and Shimizu et al. (1995) and Ciobanu et al. (2002)
Oravita, Romania Skarn (*Cretaceous*)	ORV4B	Gn–Cp–Py–Sp	–	Gheorghitescu (1975) and Cioflica and Vlad (1981) and Constantinescu et al. (1988)
Kapp Mineral, Norway SEDEX (*Late Precambrian*?)	Kmi2a Kmi5	Gn–Cp–Py Gn–Sp–Py	Very weakly metamorphosed	Flood (1967)
Mt. Isa, Australia SEDEX (*Proterozoic*)	5985C1	Sp–Gn–Py–Po–Ss	Greenschist facies Large et al. (2005)	Mathias and Clark (1975) and Perkins (1997) and Painter et al. (1999)
Bleikvassli, Norway Recrystallized SEDEX (*Ordovician*)	Bv-1 V598572	Py–Sp–Gn–Cp–Po Cp–Ap–Gn–Sp–Po–Ss	Upper amphibolite-lower granulite facies (570 °C, 7.5–8 kbar) Cook (1993); Rosenberg et al. (1998)	Vokes (1963, 1966) and Cook et al. (1998)
Broken Hill, Australia Recrystallized SEDEX (*Proterozoic*)	BH73 BH218	Sp–Gn–Cp–Po–Ss Gn–Sp–Po–Cp–Ss–Ac	Granulite facies (750–800 °C, 5–6 kbar)Bryndzia et al. (1990); Phillips (1981)	Haydon and McConachy (1987) and Parr and Plimer (1993) and Plimer (2007) and Spry et al. (2008)
Mofjellet, Norway Recrystallized SEDEX (*Palaeozoic*)	Mo2	Py–Gn–Sp–Cp–Po	Amphibolite facies (550 °C, 7 kbar?)Bjerkgård et al. (2001)	Saager (1967) and Cook (2001)

Mineral abbreviations: Gn = galena, Sp = sphalerite, Cp = chalcopyrite, Py = pyrite, Po = pyrrhotite, Ap = arsenopyrite, Ss = (Cu,Ag)–(Pb)–(Bi,Sb)–sulphosalts, Ac = acanthite, Tet = tetrahedrite–tennantite, St = stibnite.

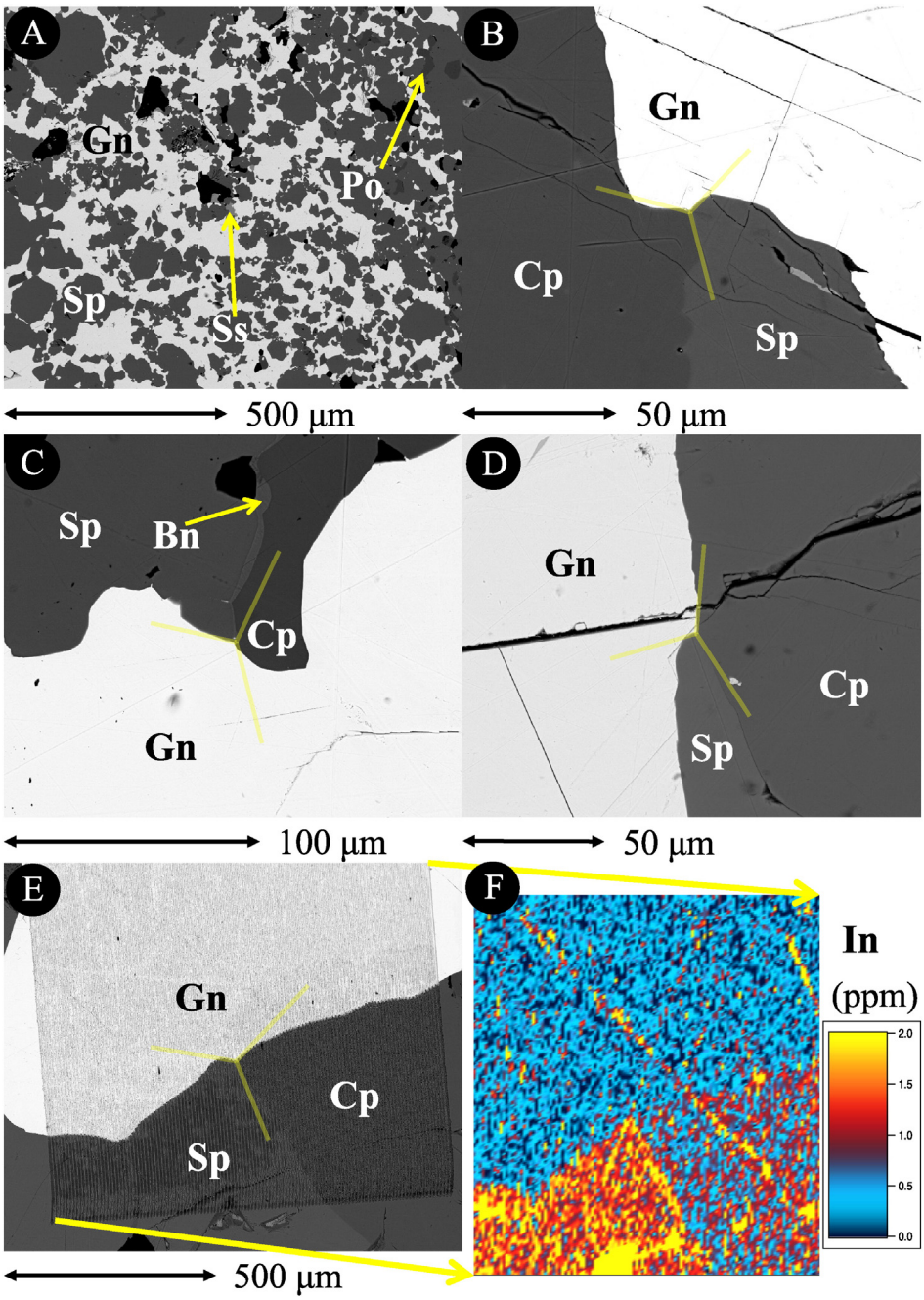

Fig. 1. Back-scattered electron images illustrating textural evidence for BMS co-crystallization. (A) Co-deposited sphalerite (Sp) and galena (Gn) in SEDEX horizon from Mt. Isa. Po = pyrrhotite, Ss = sulphosalt. (B, C, D, E) ~120° triple-junction grain boundaries between sphalerite, galena and chalcopyrite (Cp) at Herja, Baita Bihor, Bleikvassli and Broken Hill, respectively. Bn = bornite. Note grain boundaries curving towards the triple junction in order to approximate 120°. The grid in (E) has been mapped by LA-ICP-MS. (F) LA-ICP-MS element map for In corresponding to the area indicated in (E).

GLITTER data reduction software (Van Achterbergh et al., 2001). Significant effort was invested using GLITTER off-line to recognise the presence of inclusions by careful visual inspection of multi-element concentration patterns in each time-resolved depth profile. If obvious inclusions were present (e.g. by interdependencies of Ag and Te, suggestive of hessite inclusions in galena), these analyses were either discarded or the integrated time intervals restricted to inclusion-free portions of the ablation profile. We accept that our manual approach to identifying including-related analyses is imperfect and may permit the smallest inclusions to be missed. We nevertheless emphasize that very thorough examination by SEM prior to analysis and detailed mineralogical knowledge of each sample are sound preventative measures to avoid this.

The MASS-1 standard (formerly PS-1; Wilson et al., 2002) has a Fe–Zn–Cu–S matrix in which the concentrations of these elements are sufficiently close to natural sphalerite and chalcopyrite to allow for adequate calibration of sphalerite and chalcopyrite analyses. Even if Wilson et al. (2002) specifically mention that MASS-1 is not well suited for analysis of galena, we do not believe the small amount of Pb contained within MASS-1 compared to galena poses a significant problem for quantification in this study as discussed in George et al. (2015). We have chosen to consider MASS-1 homogeneous even if suggestions

of possible heterogeneity in the particle size of sulphide phases in MASS-1 have recently circulated. We have also chosen, for the purpose of the present work, to accept the trace element concentrations given in the latest MASS-1 certificate of analysis (available on the United States Geological Survey website). This may carry implications for some elements given the significant differences in concentration values compared to those given by Wilson et al. (2002) in the original paper. Irrespective of absolute concentrations, however, we have every confidence that the relative trends identified below are fully correct. As per the updated certificate of analyses for MASS-1, no value for Ge is given, precluding quantification of Ge concentrations from LA-ICP-MS analysis.

5. Results

Of the twenty-four elements analysed, seventeen were found to be present at measurable concentrations and could be quantified within sphalerite, galena or chalcopyrite (Table 3). These common 17 elements can be categorized into 3 groups based on their observed partitioning behaviours with respect to sphalerite, galena and chalcopyrite.

Group 1 elements include Mn, Fe, Zn, As, Se, Ag, Cd, Sb, Te, Tl and Bi. These elements are consistently concentrated within the same sulphide in all examined samples. Some elements also have clear secondary hosts.

Group 2 elements are Ga and In. These elements are primarily concentrated in sphalerite in samples that have not been recrystallized, whereas the concentration of these elements in chalcopyrite is high in recrystallized samples. This usually makes chalcopyrite the primary host of Ga, and occasionally of In, in recrystallized deposits.

Group 3 elements are Co, Cu and Hg. These elements display a generally predictable partitioning trend, usually preferentially incorporated within sphalerite. This trend is, however, not observed in all samples. Table 4 summarizes these trends, showing each trace element with its corresponding BMS host(s).

Tin does not fit neatly into any of the three groups. It displays behaviour similar to Group 2 elements; the concentration of Sn in chalcopyrite is higher in recrystallized samples such that chalcopyrite is usually the primary host. However, in samples that have not recrystallized, Sn may be primarily concentrated in sphalerite, galena or chalcopyrite.

Measured concentrations of Au were, in many cases, below minimum limits of detection, and are not included in our tabulated dataset. Despite this, there is published evidence for BMS hosting invisible gold, notably in seafloor sulphides (e.g., Bortnikov et al., 2000; Cabri et al., 2000).

LA-ICP-MS trace element maps representative of base metal ores formed at equilibrium in skarn, epithermal, recrystallized and primary SEDEX deposits are shown as Figs. 2-8, respectively. These visually illustrate the preferred BMS hosts for various trace elements in a range of deposits that, with the exception of skarns, are typical of base metal ores. The maps test the validity of the above-defined groups of elements for deposits of contrasting ages, spanning Neogene to Precambrian, and of different tectonic setting, varying from magmatic-hydrothermal systems in younger terranes to metamorphosed epigenetic ores in older orogens and cratons. The maps are thus relevant for the intrinsic variability in physiochemical conditions of ore formation in each specific case, and also across their representative deposit types.

Fig. 2 shows trace element distributions in a sphalerite–galena assemblage hosted by garnet skarn from the proximal Antoniu orepipe at Baita Bihor which exemplify preferential partitioning of elements in each sulphide according to the rules in Groups 1 and 3, i.e., sphalerite primarily hosts Fe, Cd, Mn, In, Co and Cu, whereas galena hosts Ag, Bi, Sb, Se, Te and Tl. The caries-like textures are indicative of the equilibrium conditions between the two sulphides. Low levels of Se are noted in sphalerite, whereas galena hosts low levels of Fe, Cd and Cu. Grain-scale zoning of Se is recognised within galena, as are Fe and Mn within sphalerite. Copper concentrations in sphalerite are sporadic, consistent with the presence of chalcopyrite disease. There also appears to be a fracture in galena highlighted by high concentrations of Cu.

A galena-sphalerite assemblage with similar carries texture but hosted within marble from the distal Marta orepipe at Baita Bihor reveals comparable trace element distributions (Fig. 3). Iron, Cd, Mn, In and Co are all primarily concentrated within sphalerite, whereas Ag, Bi, Sb, Se, Te and Tl are all primarily concentrated in galena. Moderate concentrations of Ga and Se are noted in sphalerite, and some Cd is present in galena. Both Fe and Mn display erratic distributions within sphalerite, which may be indicative of micro-inclusions, zonation or both. Fractures present in sphalerite concentrate high levels of Sb, Mn and In.

Trace element distributions in tri-component sulphide assemblages formed at equilibrium in skarn is demonstrated by sphalerite–galena–chalcopyrite association at Oravita (Fig. 4). Sphalerite primarily hosts Cd, Mn, In, Sn and Ga, with each of these elements zoned to some extent. The zonation patterns displayed by In, Sn and Ga appear to match closely, whereas Cd distributions are inversed to those for Mn. A splay of fractures near the boundary between sphalerite and chalcopyrite, concentrate Ag, Bi, Sb, Se, Te, Tl and Fe. Apart from these fractures, all these elements (excluding Fe) are primarily hosted in galena, although Sb concentrations are low and are matched closely by chalcopyrite. Low levels of Cd are also noted in galena. Notable is that, compared to sphalerite and galena, chalcopyrite is relatively barren with respect to trace elements.

Epithermal ore also comprising tri-component assemblages (sphalerite–galena–chalcopyrite) from Toroiaga shows trace element distributions that are comparable with those in the skarn at Oravita (Fig. 5). Iron, Cd, Mn, In and Ga are all primarily hosted by sphalerite and In is zoned at this spatial resolution. Silver, Bi, Sb, Se, Te and Tl are all hosted by galena, whereas moderate amounts of Cd are also noted. There is however an increase in Sb in the epithermal ore. Notable here is also that, whereas Sn is distributed quite evenly across both galena and chalcopyrite on the map, spot analysis (Table 3) reveals that galena is the primary host. Indium is also present in chalcopyrite. Galena is clearly zoned with respect to Bi, with highest concentrations at the grain rim.

Fig. 6 shows trace element distributions in a co-crystallized sphalerite–galena assemblage from Broken Hill where all elements are concentrated by their preferred host. Sphalerite primarily hosts Co, Cd, Mn, In, Ga and Cu whereas galena concentrates Ag, Bi, Sb, Se, Tl and Sn. Modest amounts of In are apparent in galena; low levels of Cd and Cu are also present. Galena displays weak zoning with respect to Ag and Sb; the absolute concentrations of both elements decrease away from what appears to be fractures.

Fig. 7 reveals the trace element distributions in a sphalerite–galena–chalcopyrite assemblage from the Bleikvassli recrystallized SEDEX deposit that are comparable to tri-component assemblages from skarn and epithermal ores. Here, however, Ga is primarily concentrated in chalcopyrite. Sphalerite concentrates Fe, Cd, Mn and In, whereas galena concentrates Ag, Bi, Sb, Se and Tl. Spot analysis (Table 3) shows that Sn concentrations are highest in galena, followed closely by chalcopyrite. Modest enrichment of Ag and In is noted in chalcopyrite, as well as Ga in sphalerite. There appears to be a poorly defined zonation in galena and chalcopyrite with respect to Sn.

Trace element distributions in a sphalerite–galena assemblage from the Kapp Mineral SEDEX deposit are shown in Fig. 8. Sphalerite primarily hosts Fe, Cd, Mn, In, Sn, Ga, Co, Hg and Cu, whereas galena hosts Ag, Bi, Sb, Se and Tl. The LA-ICP-MS mapping also shows low levels of As in galena. Modest amounts of Ag are noted in sphalerite.

Table 3
Trace element concentrations in sphalerite, galena and chalcopyrite determined by LA-ICP-MS spot analysis. Data in ppm (molar).

Locality	Sample/sulphide		Element																
Herja	Hj13		Mn	Fe	Co	Cu	Zn	Ga	As	Se	Ag	Cd	In	Sn	Sb	Te	Hg	Tl	Bi
Romania	Sphalerite (10)	Mean	2392	88022	76	585	IS	1.7	0.05	3.6	1.4	1045	4.4	38	0.32	0.02	0.60	0.00	0.00
		St. Dev.	362	8400	24	1150		0.48	0.05	3.6	1.8	139	9.1	51	0.63	0.03	0.06	0.00	0.00
	Galena (10)	Mean	9.0	50	0.09	5.0	19	0.18	1.1	258	1574	16	0.02	2.0	1509	10	0.06	0.21	179
		St. Dev.	4.1	26	0.17	8.3	10	0.23	0.50	289	254	4.4	0.01	1.3	299	14	0.03	0.06	343
	Chalcopyrite (10)	Mean	43	245967	3.3	IS	1120	0.06	0.04	5.0	71	3.1	0.69	3.9	0.53	0.00	0.04	0.01	0.00
		St. Dev.	11	14061	1.1		491	0.03	0.03	4.4	25	1.1	0.31	1.3	0.78	0.01	0.01	0.03	0.00
Toroiaga	TOR191																		
Romania	Sphalerite (10)	Mean	1035	70815	0.02	47	IS	1.4	1.7	1.0	0.54	4109	27	0.22	0.06	0.01	8.2	0.00	0.00
		St. Dev.	169	3795	0.02	36		0.49	0.89	0.77	0.32	481	31	0.30	0.09	0.02	4.7	0.00	0.00
	Galena (10)	Mean	7.9	55	0.17	5.4	4.5	0.07	27	56	2791	311	0.13	3.0	822	–	5.7	0.41	1687
		St. Dev.	5.5	44	0.19	3.9	3.4	0.05	21	58	2206	49	0.09	1.5	433	–	3.0	0.30	2185
	Chalcopyrite (10)	Mean	0.83	246711	0.03	IS	1451	0.22	0.46	0.75	54	17	14	11	0.30	0.01	39	0.00	0.00
		St. Dev.	0.34	9312	0.03		1020	0.10	0.21	0.71	53	11	8.2	7.4	0.23	0.02	14	0.00	0.00
	TOR197																		
	Sphalerite (10)	Mean	1004	75230	0.05	52	IS	1.3	1.6	0.74	0.39	4337	19	0.23	0.05	0.01	8.0	0.00	0.00
		St. Dev.	151	5397	0.09	44		0.62	1.3	0.58	0.16	407	15	0.24	0.10	0.01	7.0	0.00	0.00
	Galena (10)	Mean	7.6	344	0.33	6.8	11	0.37	118	828	1292	171	0.10	6.2	1321	14	4.7	0.35	190
		St. Dev.	6.9	940	0.29	2.7	12	0.51	102	727	328	26	0.04	1.7	291	4.9	3.5	0.20	119
	Chalcopyrite (10)	Mean	0.94	256250	0.02	IS	2213	0.08	0.73	0.80	94	24	8.2	4.2	0.53	0.04	95	0.00	0.00
		St. Dev.	1.2	9148	0.03		2971	0.06	0.58	0.69	59	27	1.8	1.7	0.49	0.04	41	0.00	0.00
	Emeric2																		
	Sphalerite (9)	Mean	831	62553	–	7207	IS	3.6	0.24	3.3	6.9	2657	89	0.35	0.88	–	2.3	0.00	0.01
		St. Dev.	121	8523	–	8088		0.82	0.26	1.9	6.8	309	79	0.23	1.3	–	0.37	0.00	0.01
	Galena (6)	Mean	5.0	31	0.04	7.8	28	0.08	1.8	–	2177	37	0.06	1.4	1756	63	0.07	0.84	863
		St. Dev.	2.5	4.1	0.04	7.1	18	0.11	1.1	–	391	4.7	0.04	0.70	391	10	0.04	0.53	536
	Chalcopyrite (9)	Mean	15	266804	–	IS	5790	1.3	0.16	11.0	41	24	13	16	4.2	–	0.39	0.00	0.05
		St. Dev.	10	16234	–		3115	0.94	0.19	7.8	25	9.4	5.2	9.5	3.5	–	0.46	0.00	0.07
Baita Bihor	BBH16B																		
Romania	Sphalerite (10)	Mean	358	1525	285	616	IS	0.62	0.04	2.4	0.25	1634	7.8	0.20	0.01	0.04	1.4	0.00	0.11
		St. Dev.	122	764	6.6	640		0.30	0.03	2.2	0.18	79	0.91	0.12	0.01	0.05	0.12	0.00	0.24
	Galena (10)	Mean	4.6	103	0.20	13	53	0.06	1.7	343	813	41	0.03	0.52	2.1	–	0.01	2.6	844
		St. Dev.	4.3	74	0.52	12	47	0.15	1.8	468	71	15	0.03	0.29	1.7	–	0.00	0.37	112
	BBH20																		
	Sphalerite (10)	Mean	3218	10333	192	27	IS	0.22	0.09	4.2	0.08	1842	3.9	0.05	0.19	0.02	1.2	0.00	0.01
		St. Dev.	525	599	10	30		0.16	0.06	3.2	0.01	118	0.42	0.02	0.38	0.04	0.19	0.00	0.01
	Galena (10)	Mean	12	110	0.17	65	39	0.06	2.7	322	3383	71	0.02	1.2	18	411	0.06	8.4	4619
		St. Dev.	6.7	96	0.29	50	17	0.10	2.5	561	368	20	0.01	0.92	9.3	65	0.04	2.0	248
	BB55																		
	Galena (10)	Mean	74	139	0.14	527	32	0.04	2.1	395	19986	156	0.21	2.4	90	–	0.02	15	38096
		St. Dev.	133	103	0.23	615	4.8	0.08	1.3	–	7159	233	0.59	1.7	245	–	0.02	2.1	60466
	Chalcopyrite (10)	Mean	31	224552	69	IS	523	0.04	0.35	4.6	22	5.1	42	47	0.28	0.05	0.02	0.02	0.36
		St. Dev.	77	11508	134		149	0.03	0.45	2.3	49	5.2	3.5	7.2	0.41	0.05	0.01	0.03	0.78
	BBH32																		
	Sphalerite (10)	Mean	1608	6558	241	15.0	IS	1.5	0.67	6.0	0.13	2834	7.0	0.20	0.20	0.02	2.4	0.00	0.01
		St. Dev.	335	1037	21	7.9		3.1	0.54	4.1	0.04	69	1.6	0.44	0.42	0.02	2.7	0.00	0.01
	Galena (10)	Mean	19	116	0.12	4.1	1.7	0.13	10	443	3694	167	0.01	0.24	33	475	11	6.4	4410
		St. Dev.	34	253	0.09	2.5	1.2	0.11	2.7	135	173	41	0.01	0.11	8.6	121	4.7	1.0	546
Oravita	ORV4B																		
Romania	Sphalerite (10)	Mean	551	1841	0.02	1490	IS	14	0.71	4.5	4.1	1409	1.6	1.3	0.04	0.06	3.3	0.00	0.37
		St. Dev.	215	314	0.04	305		11	0.44	3.1	2.2	121	3.9	2.2	0.08	0.11	2.0	0.00	0.49
	Galena (10)	Mean	2.5	17	0.07	4.4	1.6	0.07	8.6	1155	856	39	0.01	0.22	1.3	175	24	0.47	956
		St. Dev.	3.2	8.6	0.06	3.8	1.3	0.05	7.6	261	214	6.0	0.00	0.17	1.0	38	15	0.11	267
	Chalcopyrite (10)	Mean	0.12	249624	0.00	IS	6.6	0.23	0.54	8.1	0.44	0.13	0.37	0.16	0.13	0.14	2.9	0.03	1.2
		St. Dev.	0.16	7350	0.00		1.7	0.10	0.60	10	0.37	0.09	0.40	0.11	0.10	0.12	1.4	0.09	0.72
Kapp Mineral	Kmi2a																		
Norway	Galena (10)	Mean	2.4	46	0.17	7.4	4.8	0.16	8.7	300	129	39	0.02	0.41	46	–	5.7	0.07	96
		St. Dev.	1.6	34	0.08	6.4	2.7	0.14	6.0	194	38	13	0.01	0.27	14	–	5.7	0.02	53
	Chalcopyrite (10)	Mean	241	261971	0.42	IS	194	0.13	1.2	13	90	1.6	0.64	6.4	13	0.02	32	0.02	4.0
		St. Dev.	493	13155	0.87		80	0.04	1.4	29	33	1.2	0.21	1.6	7.7	0.02	40	0.01	10
	Kmi5																		
	Sphalerite (10)	Mean	5.7	10619	5.0	250	IS	2.5	0.07	2.2	18	253	0.76	8.1	0.69	0.01	7.0	0.00	0.01
		St. Dev.	1.9	1788	1.7	224		3.9	0.06	1.2	9.5	22	0.33	11	0.79	0.02	0.75	0.00	0.00
	Galena (10)	Mean	3.9	77	0.17	6.8	54	0.07	1.6	20	192	4.9	0.02	0.69	254	–	0.01	0.03	7.1
		St. Dev.	1.9	33	0.36	5.4	53	0.14	0.75	11	31	3.7	0.01	0.70	39	–	0.02	0.01	2.6
Mt. Isa	5985C1																		
Australia	Sphalerite (5)	Mean	116	38989	0.16	15	IS	2.0	3.4	0.70	3.0	1351	7.0	0.11	1.8	0.02	10	0.01	0.00
		St. Dev.	15	1062	0.04	1.5		1.2	1.3	0.54	1.1	54	0.12	0.12	0.86	0.02	5.4	0.01	0.00
	Galena (4)	Mean	5.4	224	0.25	6.4	4.3	0.13	1700	4.6	499	86	0.21	2.1	748	0.27	7.1	14	3.4
		St. Dev.	3.1	361	0.28	2.5	1.9	0.19	846	0.73	122	154	0.37	0.49	146	0.18	4.4	3.1	0.09
Bleikvassli	Bv–1																		
Norway	Sphalerite (10)	Mean	255	51984	0.05	48	IS	13	0.17	2.2	1.0	509	23	1.5	0.41	0.01	4.0	0.01	0.00
		St. Dev.	102	1134	0.04	7.4		0.75	0.19	1.5	1.1	20	0.51	1.1	0.79	0.02	0.18	0.01	0.01

(continued on next page)

Table 3 (*continued*)

Locality	Sample/sulphide		Element															
	Galena (10)	Mean	3.8	82	0.10	6.7	26	0.27	1.6	9861	1093	8.2	1.0	290	966	0.26	0.09	130	534
		St. Dev.	4.3	72	0.22	3.2	20	0.56	0.56	24503	161	6.2	0.30	87	209	0.84	0.08	6.8	41
	Chalcopyrite (5)	Mean	1.8	224617	0.01	IS	261	16	0.03	1.3	254	0.34	7.5	275	2.8	0.00	0.09	0.14	0.01
		St. Dev.	1.7	5678	0.02		46	9.1	0.01	1.1	125	0.10	1.4	221	1.6	0.01	0.07	0.15	0.01
	V598572																		
	Sphalerite (5)	Mean	1766	49536	0.35	28	IS	2.8	0.28	8.1	0.18	778	20	0.47	0.09	0.00	7.3	0.00	0.01
		St. Dev.	137	684	0.08	3.3		1.6	0.21	3.3	0.04	15	2.6	0.15	0.08	0.00	1.0	0.00	0.00
	Galena (10)	Mean	6.3	65	0.06	8.0	13	0.06	4.8	172	1042	26	0.32	98	309	–	0.04	62	1312
		St. Dev.	4.4	80	0.08	5.2	2.9	0.08	2.5	102	102	7.1	0.11	19	170	–	0.03	8.4	129
	Chalcopyrite (9)	Mean	47	221422	0.23	IS	344	1.1	0.24	7.8	5.2	2.3	10	393	1.2	0.05	0.19	0.01	0.01
		St. Dev.	10	13003	0.48		49	0.66	0.40	5.8	1.7	1.2	1.5	73	2.4	0.07	0.09	0.01	0.01
Broken Hill	BH73																		
Australia	Sphalerite (10)	Mean	16606	90076	128	71	IS	2.6	0.05	1.7	0.82	884	0.69	0.21	0.04	0.03	0.86	0.00	0.00
		St. Dev.	633	2537	10	3.2		0.12	0.04	1.0	0.27	24	0.01	0.07	0.04	0.02	0.05	0.00	0.00
	Galena (10)	Mean	36	73	0.09	2.6	16	0.09	1.3	32	249	13	0.15	39	631	0.24	0.05	0.43	4.0
		St. Dev.	17	45	0.06	1.4	8.1	0.08	0.61	20	72	3.5	0.04	5.2	615	0.33	0.04	0.11	0.77
	Chalcopyrite (5)	Mean	196	235552	1.3	IS	550	3.9	0.05	1.6	473	0.74	0.70	119	3.1	0.03	0.01	0.02	0.00
		St. Dev.	253	8084	1.1		242	0.86	0.01	0.22	110	0.68	0.10	20	3.6	0.03	0.01	0.03	0.00
	BH218																		
	Sphalerite (10)	Mean	1420	61926	47	33	IS	4.8	0.05	2.0	0.71	688	1.4	0.14	0.08	0.03	0.55	0.00	0.01
		St. Dev.	35	2316	7.8	14		0.58	0.02	1.2	0.75	30	0.05	0.13	0.10	0.05	0.06	0.00	0.02
	Galena (10)	Mean	2.3	65	0.12	3.9	30	0.05	2.2	93	237	10	0.21	72	57	–	0.05	0.09	35
		St. Dev.	1.4	44	0.11	3.4	33	0.14	2.0	167	336	5.8	0.05	8.7	107	–	0.04	0.02	2.6
Mofjellet	Mo2																		
Norway	Sphalerite (10)	Mean	460	25051	0.10	4.3	IS	0.39	0.65	2.9	0.65	1156	0.76	0.02	0.08	0.01	23	0.00	0.02
		St. Dev.	43	2452	0.05	1.0		0.09	0.46	1.1	1.2	34	0.08	0.02	0.13	0.01	8.7	0.00	0.05
	Galena (10)	Mean	2.3	33	0.12	7.5	4.6	0.14	17	319	1116	100	0.01	0.51	1750	39	333	0.33	124
		St. Dev.	1.7	10	0.07	5.6	3.0	0.07	4.6	59	348	33	0.01	0.37	325	6.0	326	0.06	24

IS: This element was used as the internal standard; Zn in sphalerite, Cu in chalcopyrite and Pb in galena.
The 17 elements displayed were commonly detected above the mdl in sphalerite, galena or chalcopyrite. S, Ni, Mo, W and Pb were measured but are not commonly detected as trace elements. Ge could not be quantified (see text). Au was measured but found to be below minimum detection limit in the majority of analysed spots. We choose not to present these data given the high levels of uncertainty and concerns about the homogeneity of Au in the MASS-1 standard (Wilson et al., 2002).
(X) = number of individual spot analyses on that sulphide in that sample. Dash = insufficient data to perform calculation (all analyses <mdl). Other <mdl values were treated as mdl/2.
*Ag concentration in galena in BH73 reduced due to secondary leaching post recrystallization (see text).

Indium, Sn and Ga all appear to be zoned in the same way within sphalerite; Bi distributions in galena are patchy.

6. Discussion

6.1. External factors on trace element partitioning

The rich exotic trace element signature of the BMMB is well documented, in particular in the Baita Bihor skarn system, where Bi, Ag, W, Se, Te, Ni, Co and Sn are all present, and are primarily concentrated within Pb-(Cu,Ag)-Sb- or Bi-sulphosalts, and as Bi- and Ag-tellurides and selenides (Cioflica et al., 1995; Cioflica et al., 1997; Ilinca et al., 2012; Ciobanu et al., 2014). It has, however, recently been shown that many of these trace elements are also present at high concentrations within common sulphides (e.g., galena; George et al., 2015). Oravita, located approximately 350 km from Baita Bihor, has a similar geochemical signature as a consequence of related ore fluids associated with Late Cretaceous calc-alkaline magmatism. From these two deposits, it is possible to directly compare the partitioning behaviour of trace elements between co-crystallizing BMS in skarns formed from similar hydrothermal fluids at high temperature (~>450 °C) conditions proximal to a porphyry granitoid-derived source of fluids (Baita Bihor, Antoniu orepipe; Fig. 2), low temperature (~<200 °C) conditions distal to a porphyry hosted in carbonate (Baita Bihor, Marta orepipe; Fig. 3), and a shallow Cu skarn satellite to a porphyry (Oravita; Fig. 4). In each case, the trace element distributions in the BMS assemblages from these systems are almost identical; all Group 1 and 2 trace elements present are primarily hosted in the same minerals (Fe, Cd, Mn, In, Sn, Ga, Co and Cu in sphalerite, Ag, Bi, Sb, Se, Te and Tl in galena).

Similar to the BMMB, both the Toroiaga and Herja epithermal systems in the Baia Mare District, Romania, boast similar geochemical signatures expressed in part by the presence of Pb–Ag–Sb–As or lesser -Bi sulphosalts. This is a result of their common association with relatively young magmatic-hydrothermal systems, which produced comparable ore fluids at both deposits. Despite the similarities however, Toroiaga is a relatively deep system, crystallizing BMS at high temperatures (~<400 °C; Cook, 1997), whereas Herja is shallow and relatively cool (~<200 °C; Borcos et al., 1975). Thus Toroiaga (Fig. 5) and Herja (see

Table 4
Base metal sulphide hosts of various trace elements as determined from LA-ICP-MS analysis.

Trace element	Mn	Fe	Co	Cu	Zn	Ga	As	Se	
Primary BMS host	Sp[1]	Sp>Gn[1]	Sp>Cp[3]	Sp>Gn[3]	Cp[1]	Sp[2]	Gn>Sp[1]	Gn[1]	
Trace element	Ag	Cd	In	Sn	Sb	Te	Hg	Tl	Bi
Primary BMS host	Gn[1]	Sp>Gn[1]	Sp>Cp[2]	?[*]	Gn>Cp[1]	Gn[1]	Sp>Cp[3]	Gn[1]	Gn[1]

Abbreviations: BMS = base metal sulphide. Sp = sphalerite, Gn = galena, Cp = chalcopyrite.
[1] Group 1 elements. Trend observed in all examined samples.
[2] Group 2 elements. Recrystallization increases element concentration in Cp and may make Cp primary host.
[3] Group 3 elements. Trend generally, yet not always, true.
[*] Recrystallization increases Sn concentration in Cp such that Cp is usually primary host in recrystallized samples. Below recrystallization conditions, no trend is observed.

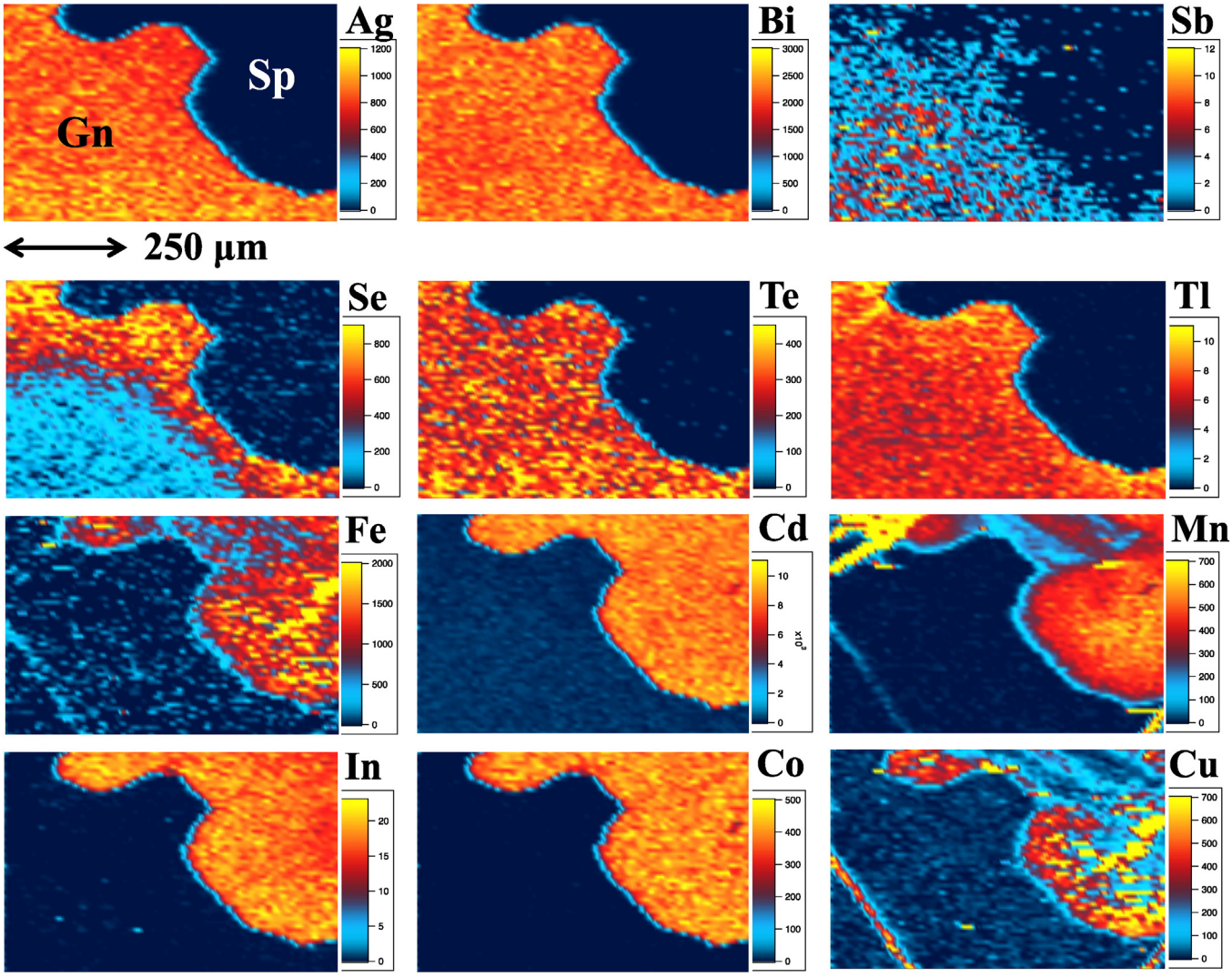

Fig. 2. LA-ICP-MS element maps (Ag, Bi, Sb, Se, Te, Tl, Fe, Cd, Mn, In, Co, Cu) of an assemblage comprising co-crystallized sphalerite (Sp) and galena (Gn) from the Antoniu orepipe, Baita Bihor skarn deposit (sample BBH16B). Note preferential concentration of Fe, Cd, Mn, In, Co and Cu in sphalerite and of Ag, Bi, Sb, Se, Te and Tl in galena. Concentration scales in parts-per-million (weight).

figure 6 in George et al., 2015) allow direct comparison of the partitioning behaviour of trace elements between two epithermal systems with similar ore fluids yet different physical conditions of ore formation. In both systems, trace element distributions in the BMS assemblages are almost identical; all Group 1 and 2 trace elements present are primarily hosted in the same BMS phase.

Even higher temperatures and pressures only slightly alter the primary BMS hosts. The recrystallized SEDEX Broken Hill deposit situated in the Curnamona Province, Australia, was regionally metamorphosed to granulite facies (750–800 °C, 5–6 kbar, Phillips, 1981; Bryndzia et al., 1990). This caused a complete recrystallization of the ore, allowing for pervasive re-partitioning of trace elements from the low temperature SEDEX distributions to the preferred distributions at these high metamorphic temperatures and pressures. Some have also argued that extensive melting of the BMS assemblage took place at peak metamorphic conditions (Mavrogenes et al., 2001; Frost et al., 2002, 2005). This too would cause a redistribution of trace elements as new sulphides crystallize from melt at high temperatures. Despite the granulite facies metamorphism however, Group 1 trace elements at Broken Hill are all hosted by the same BMS phases as the skarn and epithermal systems discussed above (Fig. 6). Only the primary hosts of Group 2 elements and Sn seem to be altered by the temperatures and/or pressures associated with upper amphibolite to granulite facies metamorphism. The preferred BMS host for Ga at lower temperatures is sphalerite, almost always becoming chalcopyrite in recrystallized assemblages. Despite In concentrations also increasing in chalcopyrite during recrystallization, sphalerite almost always remains the primary host. Tin exhibits a comparable relationship to Ga as chalcopyrite typically becomes the primary Sn host at high temperatures/pressures that cause recrystallization. Thus, as a result of recrystallization chalcopyrite usually contains more Sn than galena which, in turn, contains more Sn than sphalerite, so that $Sn_{chalcopyrite} > Sn_{galena} > Sn_{sphalerite}$.

Like Broken Hill, the Bleikvassli deposit (Norway) also underwent high-grade (upper amphibolite) metamorphism. Peak conditions reached 7.5–8 kbar, and 570 °C (Cook, 1993; Rosenberg et al., 1998). Despite a lower peak temperature than Broken Hill, these temperatures were still adequate for complete recrystallization of the BMS assemblage. The Bleikvassli system is oxidized, evidenced by large pyrite metablasts, and a distinct syn-metamorphic sulphidation–oxidation halo enclosing the ore (Rosenberg et al., 2000). In contrast, Broken Hill is a strongly reduced system, as evidenced by the stability of pyrrhotite, lack of pyrite, and the Eu enrichment of proximal exhalites

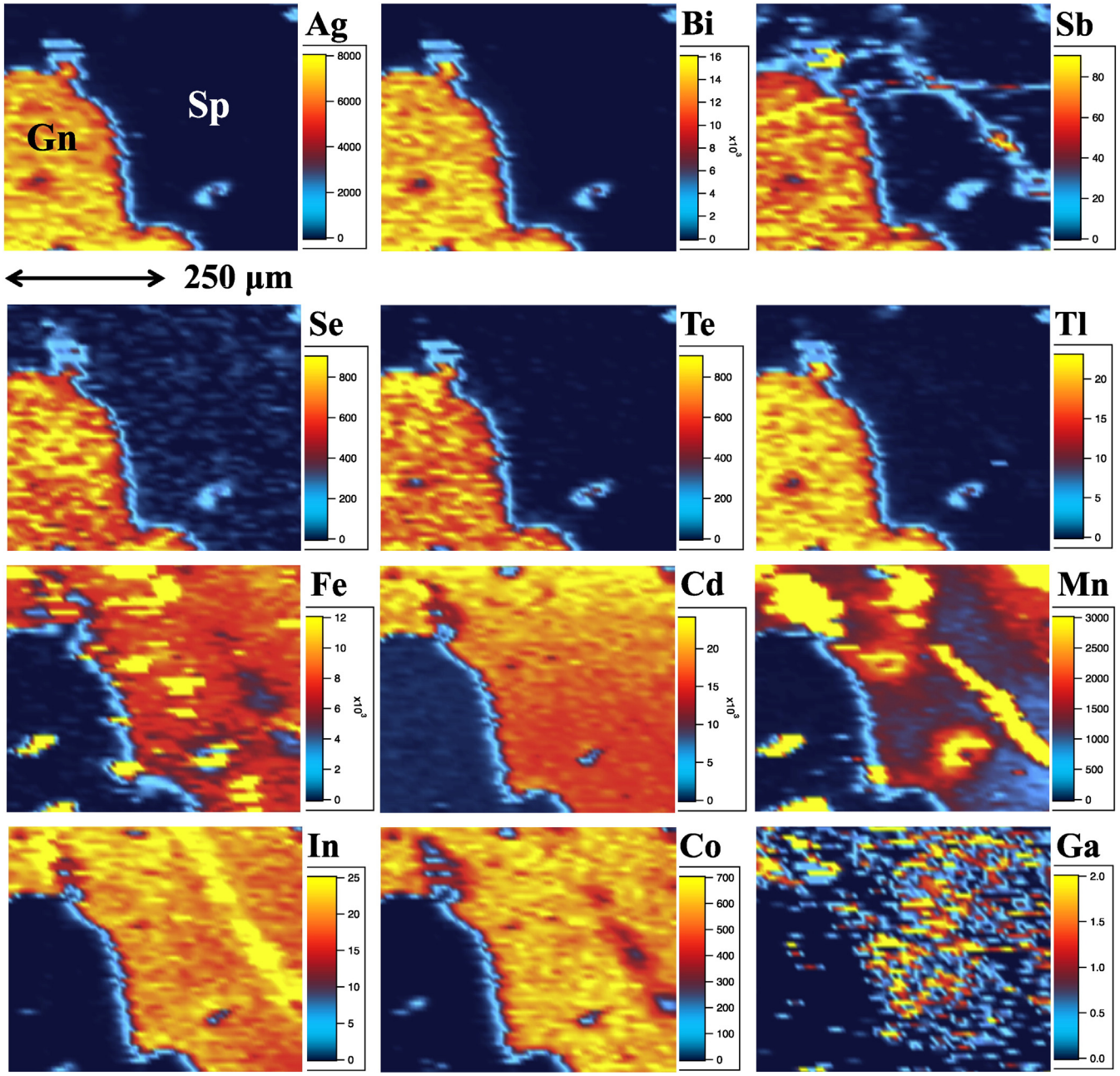

Fig. 3. LA-ICP-MS element maps (Ag, Bi, Sb, Se, Te, Tl, Fe, Cd, Mn, In, Co, Ga) of an assemblage comprising co-crystallized sphalerite (Sp) and galena (Gn) from the Marta orepipe, Baita Bihor skarn deposit (sample BBH32). Note preferential concentration of Fe, Cd, Mn, In, Co and Ga in sphalerite, and of Ag, Bi, Sb, Se, Te and Tl in galena. Concentration scales in parts-per-million (weight).

(Lottermoser, 1989; Leyh and Conor, 2000). Yet in both recrystallized SEDEX deposits, all Group 1 trace elements are hosted primarily within the same phases, galena, sphalerite and chalcopyrite (Figs. 6 and 7), strongly indicating that redox conditions have little to no effect on primary BMS hosts.

The Kapp Mineral SEDEX occurrence (Svalbard Archipelago, Norway) lacks any enhanced trace element geochemical signature such as that found in the BMMB or the Baia Mare District, and has not been significantly reworked since initial deposition. Yet despite the differences compared to deposits of more complex geochemistry and/or geological history, all Group 1 trace elements are primarily hosted by the same phases as in all other samples from all deposits, and Group 2 elements are primarily hosted by the same minerals as in all samples from non-recrystallized deposits (Fig. 8). This again strongly points to the conclusion that different ore types, deposit ages, host terrains and physiochemical conditions of ore formation do not alter the preferred host for almost all trace elements.

6.2. Intrinsic factors on trace element partitioning

The primary factors that control trace element partitioning identified in this study are intrinsic to the trace elements and BMS in question. These factors include element oxidation state, ionic radius of the substituting element, element availability and the maximum trace element budget that a given sulphide mineral can accommodate.

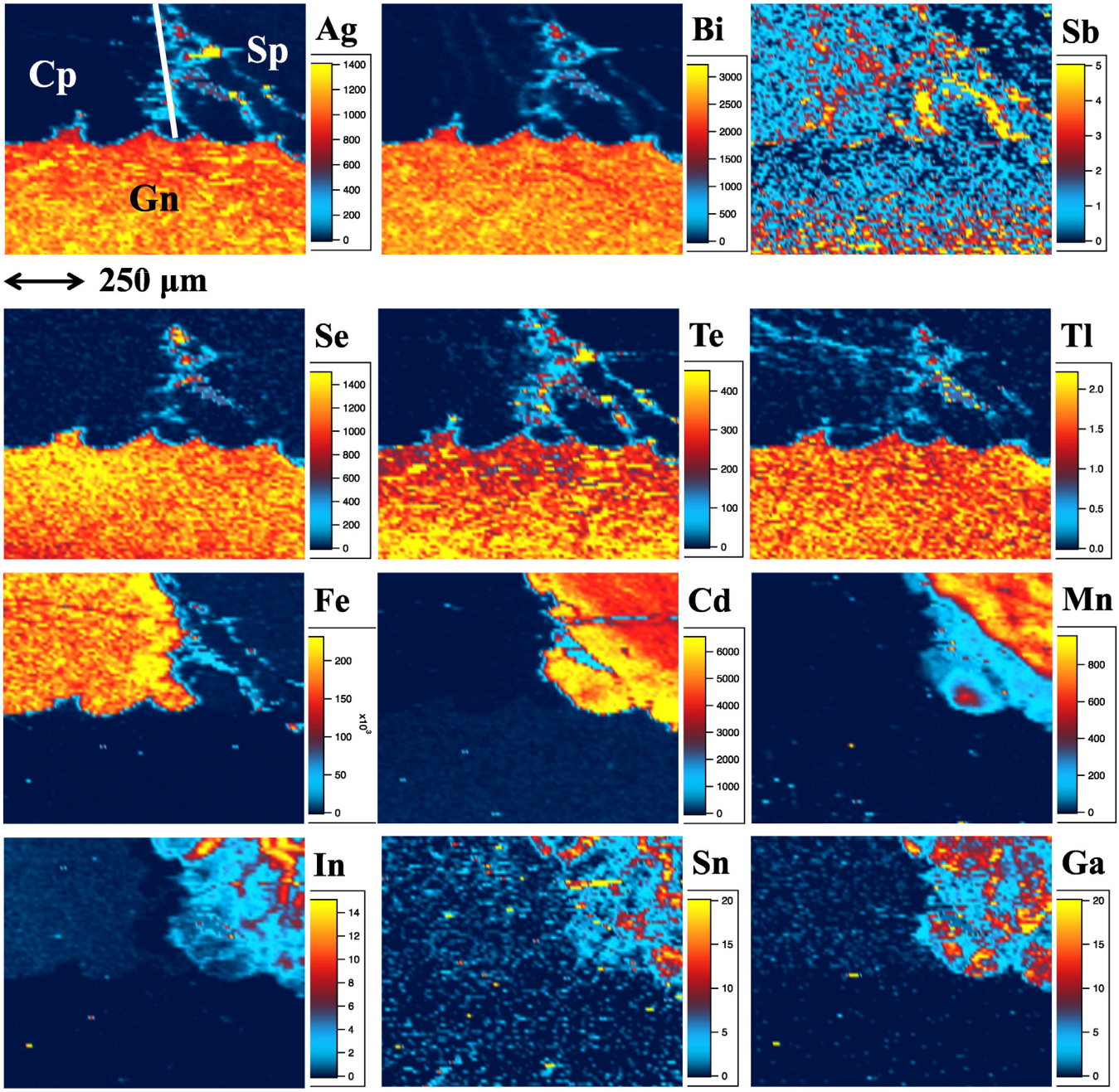

Fig. 4. LA-ICP-MS element maps (Ag, Bi, Sb, Se, Te, Tl, Fe, Cd, Mn, In, Sn, Ga) of an assemblage comprising co-crystallized sphalerite (Sp), galena (Gn) and chalcopyrite (Cp) from the Oravita skarn deposit (sample ORV4B). Note preferential concentration of Fe, Cd, Mn, In, Sn and Ga in sphalerite, of Ag, Bi, Se, Te and Tl in galena, and also the modest enrichment of Sb in galena over chalcopyrite. Concentration scales in parts-per-million (weight).

Sphalerite and galena are both ionic crystals, thus the incorporation of trace elements into them is governed by Goldschmidt's rules of substitution (Goldschmidt, 1954), and Ringwood's subsequent modifications (Ringwood, 1955). These state:

1. The ions of one element can extensively replace those of another in ionic crystals if their radii differ by less than approximately 15%.
2. Ions whose charges differ by one unit substitute readily for one another provided electrical neutrality of the crystal is maintained. If the charges differ by more than one unit, substitution is generally slight.
3. When two different ions can occupy a particular position in a crystal lattice, the ion with the higher ionic potential forms a stronger bond with the anions surrounding the site.
4. Substitutions may be limited, even when the size and charge criteria are satisfied, when the competing ions have different electronegativities and form bonds of different ionic character.

Sphalerite and galena both have simple formulae: $M^{2+}S^{2-}$, where M is Zn or Pb, respectively. All metallic trace elements considered here substitute into this M site in both minerals. Thus, as per Goldschmidt's second rule, only metals in the 1+, 2+ or 3+ oxidation state will substitute extensively into the M site. A small number of tetravalent ions may also substitute into sphalerite or galena (e.g., Ge^{4+} in sphalerite; Cook et al., 2015), although such substitutions are likely to involve the creation of lattice vacancies to maintain charge balance.

Chalcopyrite differs from sphalerite and galena in that it is not a fully ionic structure, nor is there consensus on the principal oxidation states

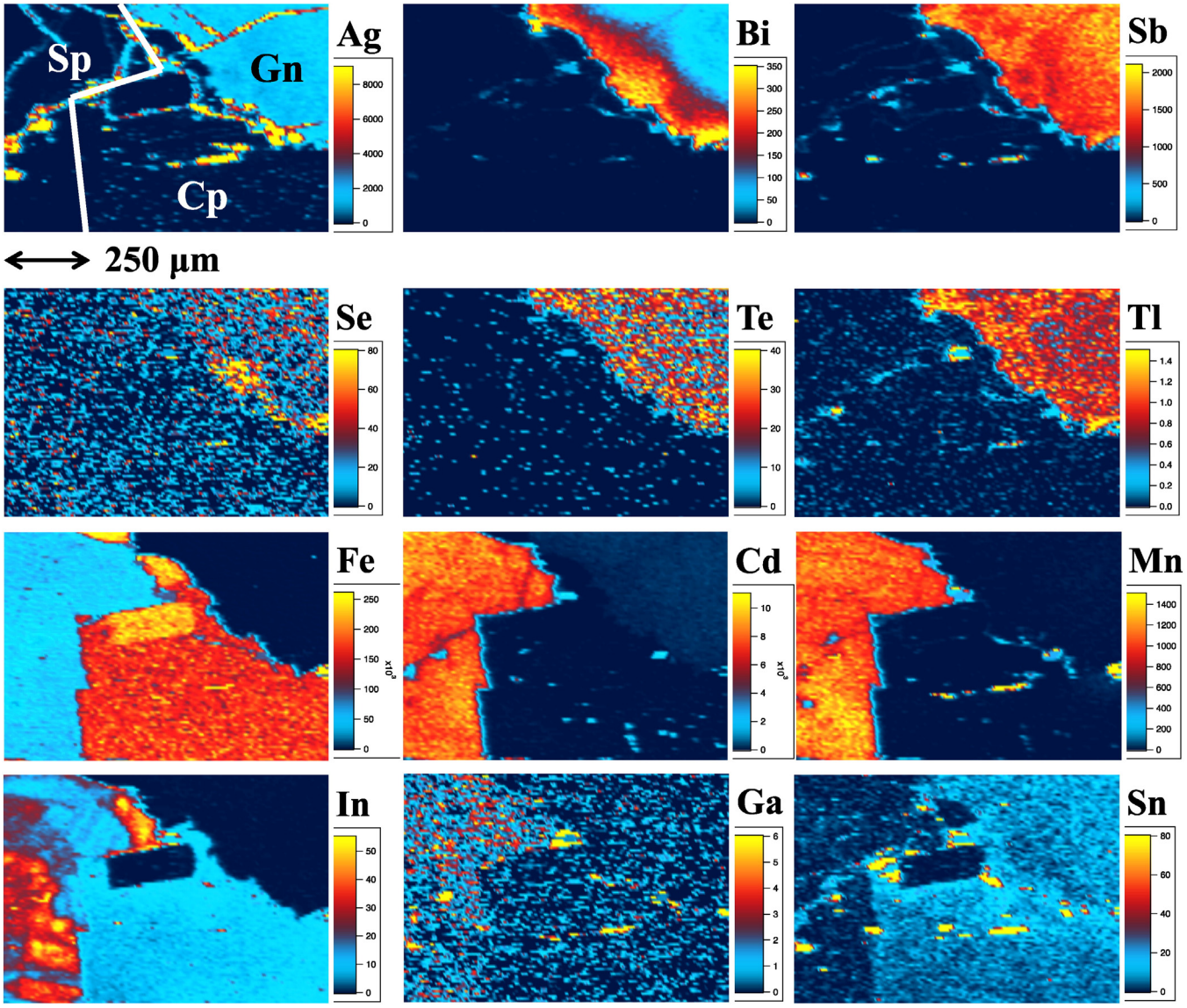

Fig. 5. LA-ICP-MS element maps (Ag, Bi, Sb, Se, Te, Tl, Fe, Cd, Mn, In, Ga, Sn) of an assemblage comprising co-crystallized sphalerite (Sp), galena (Gn) and chalcopyrite (Cp) from the Toroiaga epithermal deposit (sample TOR197). Note preferential concentration of Fe, Cd, Mn, In and Ga in sphalerite, of Ag, Bi, Sb, Se, Te and Tl in galena, and also the modest enrichment of Sn in both chalcopyrite and galena. Concentration scales in parts-per-million (weight).

of its constituents. Hall and Stewart (1973) described stereochemical evidence for a "strong covalently-bonded configuration with an effective ionic state between $Cu^{+}Fe^{3+}S^{2-}{}_{2}$ and $Cu^{2+}Fe^{2+}S^{2-}{}_{2}$". Todd and Sherman (2003), Todd et al. (2003), and Mikhlin et al. (2005) claim that the chemical structure and nominal oxidation states in chalcopyrite are $Cu^{2+}Fe^{2+}S_2^{2-}$. This was questioned by Pearce et al. (2006), who presented X-ray absorption spectroscopic (XAS) evidence that the Cu in chalcopyrite is nominally monovalent and that Fe is nominally trivalent; i.e., $Cu^{+}Fe^{3+}S_2^{2-}$. Pearce et al. (2006) also note that a nominally divalent character in copper sulphides is very rare, and energy peaks associated with Cu^{2+} can be explained by contamination by Cu^{2+} species. There is continued debate over whether the oxidation state of iron in chalcopyrite varies between Fe^{2+} and Fe^{3+}. Nevertheless, it seems trace element substitution into chalcopyrite is restricted to ions between 1+ and 4+.

For divalent metallic trace elements substituting into either sphalerite or galena, the primary factor affecting substitution is the ionic radius of the trace element and that of the corresponding Zn^{2+} or Pb^{2+} ion respectively. As per Goldschmidt's first rule, extensive substitution will take place if these ionic radii differ by less than approximately 15%. If wholly true however, this first rule seems to exclude most elements, divalent or otherwise, from substituting into either sphalerite or galena (Fig. 9A, B), despite broad evidence that many of these excluded elements are present in solid solution within these sulphides. Thus it can be assumed that at higher temperatures, elements with an ionic radius discrepancy >15% may still be substituted into an ionic lattice; indeed Goldschmidt's first rule does not take temperature into account (Philpotts, 1978).

There are several divalent transition metal ions that have ionic radii similar to Zn^{2+} (0.60 Å) in tetrahedral coordination — as in sphalerite (Fig. 9A). $Iron^{2+}$ (0.63 Å), Mn^{2+} (0.66 Å), Co^{2+} (0.58 Å) and Cu^{2+} (0.57 Å) are within 15% of the Zn^{2+} ionic radius, whereas Cd^{2+} (0.78 Å) is slightly larger than this ±15% 'window'. This provides the basis for the exceptionally high concentrations of Fe, Mn, and Cd that are often measured in sphalerite (e.g., Cook et al., 2009; Ye et al., 2011). Divalent Cu and Co may also be significantly incorporated into sphalerite, although this is usually limited due to the relative rarity of Cu^{2+} in sulphides, and the substitution of Co into Cu-(Fe)-sulphides

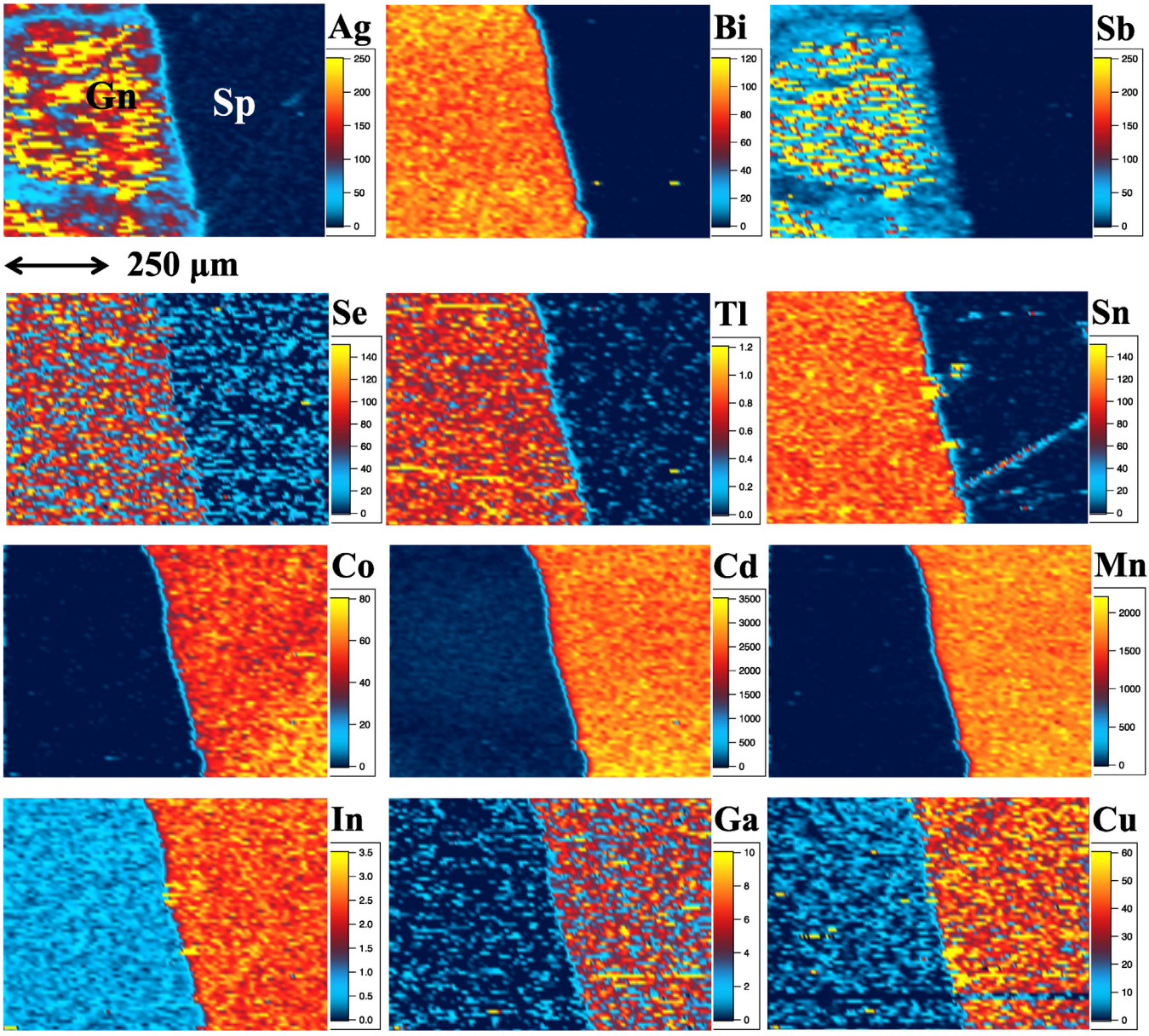

Fig. 6. LA-ICP-MS element maps (Ag, Bi, Sb, Se, Tl, Sn, Co, Cd, Mn, In, Ga, Cu) of an assemblage comprising co-crystallized sphalerite (Sp) and galena (Gn) from the Broken Hill recrystallized SEDEX deposit (sample BH218). Note preferential concentration of Co, Cd, Mn, In, Ga and Cu in sphalerite, of Ag, Bi, Sb, Se, Tl and Sn in galena, and also the modest enrichment of In in galena. Concentration scales in parts-per-million (weight).

and pyrite. Thus the presence or absence of other sulphides may significantly affect the substitution of Co into sphalerite, and this is likely the reason why Co is a Group 3 trace element; having a generally predictable partitioning trend that does not hold on all occasions. In addition, the classification of Co and Cu as a Group 3 trace elements may also reflect the tendency for these elements to be present as micro-inclusions of distinct phases in sphalerite and galena. Due to their favoured incorporation in sphalerite, galena is relatively barren of most divalent cations. However, if sphalerite is not present, or if the total number of divalent cations is greater than the trace element budget that sphalerite can accommodate, some of the surplus may substitute into galena if temperatures are high enough. This likely explains the significant amounts of Cd occasionally measured in galena (e.g., sample TOR191; Table. 3).

For metal ions that differ in charge from the 2+ oxidation state, substitution into sphalerite and galena is governed not only by ionic radius, but also the availability of other ions to participate in coupled substitutions. Fig. 9B clearly shows why galena typically hosts high concentrations of Ag and Bi, as Ag^{+} (1.15 Å) and Bi^{3+} (1.03 Å) are both within 15% of the Pb^{2+} (1.19 Å) ionic radius in octahedral coordination - as in galena. This provides the basis for the well-established coupled substitution $Ag^{+} + (Bi^{3+}, Sb^{3+}) \leftrightarrow 2Pb^{2+}$ which permits substantial incorporation of Ag and Bi into galena (Chutas et al., 2008; Renock and Becker, 2011). Due to its smaller ionic radius, substitution of Sb^{3+} (0.76 Å) tends to occur to a lesser extent than Bi^{3+}. In a similar way, ionic radius constraints restrict significant substitution of As^{3+} (0.58 Å) into galena, except perhaps at very high temperatures and in the absence of Bi and/or Sb. Incorporation of In^{3+} (0.80 Å) via the same coupled substitution together with Ag^{+} is minimal, despite the ionic radius of Pb^{2+} being closer to In^{3+} than Sb^{3+}. This is likely to be due to the preferred substitution of this ion into sphalerite, when that mineral is also present. Fig. 9A illustrates this, with the In^{3+} (0.62 Å) ion within 15% of the Zn^{2+} (0.60 Å) ionic radius in tetrahedral coordination. Similar to In^{3+}, Ga^{3+} (0.47 Å) also substitutes into sphalerite. However, in order for such substitutions to take place,

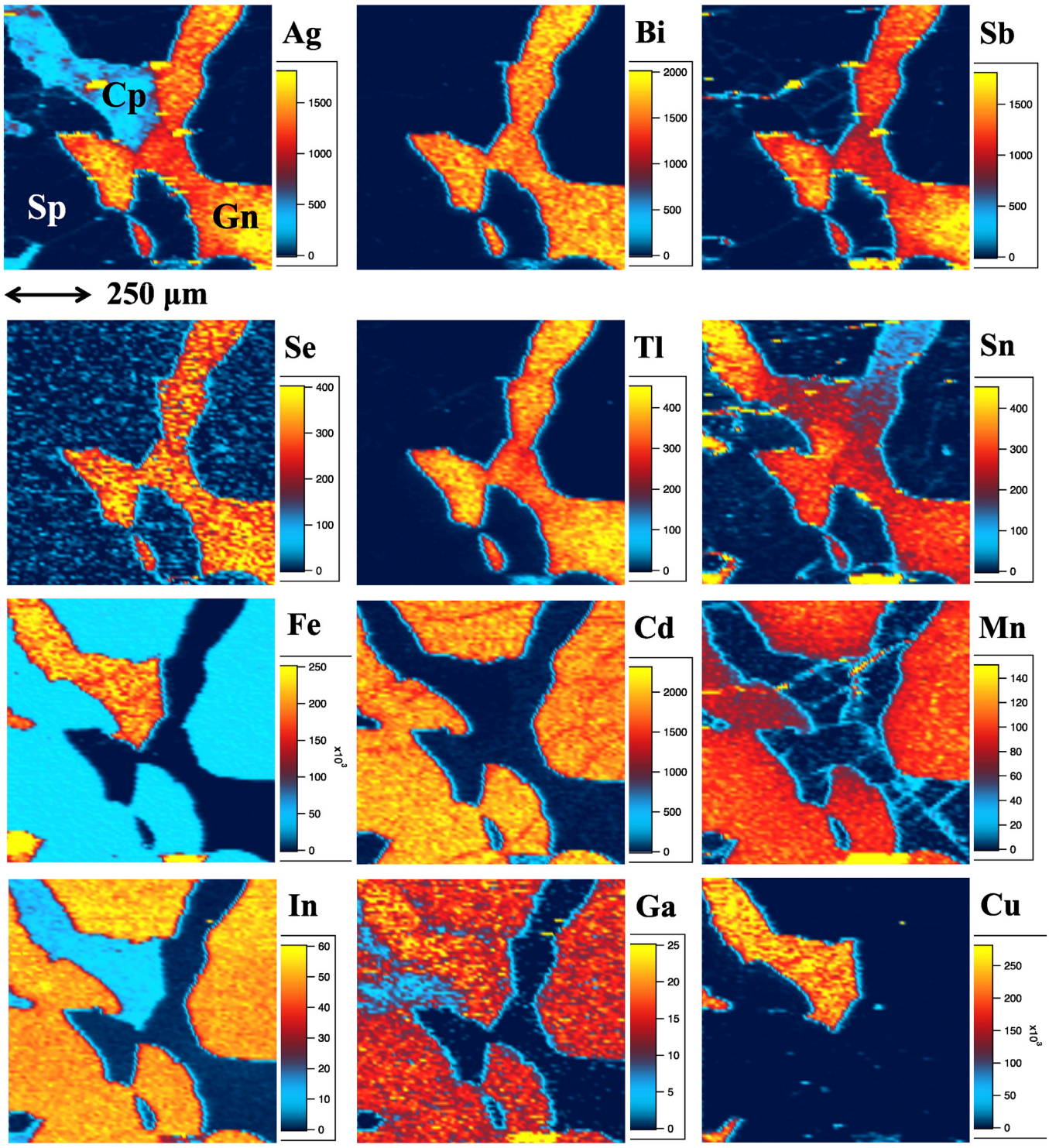

Fig. 7. LA-ICP-MS element maps (Ag, Bi, Sb, Se, Tl, Sn, Fe, Cd, Mn, In, Ga, Cu) of an assemblage comprising co-crystallized sphalerite (Sp), galena (Gn) and chalcopyrite (Cp) from the Bleikvassli recrystallized SEDEX deposit (sample Bv-1). Note preferential concentration of Fe, Cd, Mn and In in sphalerite, of Ag, Bi, Sb, Se and Tl in galena, and of Ga in chalcopyrite. Tin is distributed relatively evenly across galena and chalcopyrite. Modest amounts of Ga are noted in sphalerite, as well as Ag and In in chalcopyrite. Concentration scales in parts-per-million (weight).

a monovalent ion would be necessary to accompany these trivalent ions. Commonly, Cu^{+} (0.60 Å) plays the accompanying role (Cook et al., 2009; Cook et al., 2011b, 2012), as may Ag^{+} (1.00 Å) on rare occasions. In the absence of sphalerite, it can be assumed that In^{3+} could potentially substitute into galena, yet no supportive evidence has been found.

Small amounts of Tl^{+} and Cu^{+} may substitute into galena alongside Ag^{+} in the coupled substitution (Ag^{+}, Cu^{+}, Tl^{+}) + (Bi^{3+}, Sb^{3+}) ↔ $2Pb^{2+}$ (George et al., 2015). Fig. 9B shows that Tl^{+} (1.50 Å) is likely to be preferred over Cu^{+} (0.77 Å) in this substitution as it is closer in ionic radius to Pb^{2+} (1.19 Å) in octahedral coordination. Conversely, the Cu^{+} ion in tetrahedral coordination is much closer to the ionic radius

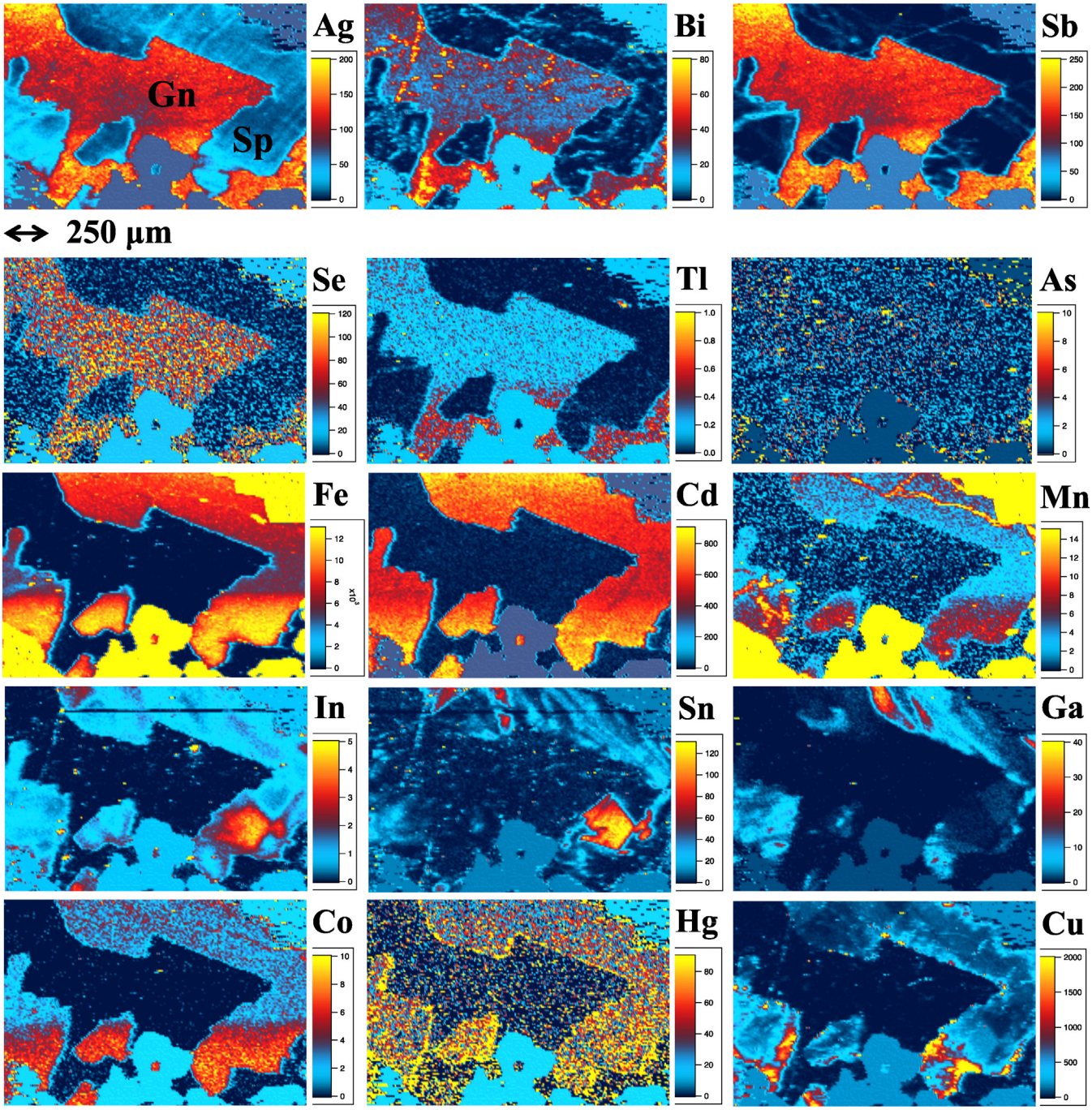

Fig. 8. LA-ICP-MS element maps (Ag, Bi, Sb, Se, Tl, As, Fe, Cd, Mn, In, Sn, Ga, Co, Hg, Cu) of an assemblage comprising co-crystallized sphalerite (Sp) and galena (Gn) from the Kapp Mineral SEDEX deposit (sample Kmi5). Note preferential concentration of Ag, Bi, Sb, Se and Tl in galena, of Fe, Cd, Mn, In, Sn, Ga, Co, Hg and Cu in sphalerite, and also a slight enrichment of As in galena. Concentration scales in parts-per-million (weight).

of Zn^{2+} (Fig. 9A), and as such, would be preferentially incorporated into sphalerite via the coupled substitution $Cu^{+} + X^{3+} \leftrightarrow 2Zn^{2+}$, where trivalent X is commonly In. Higher concentrations of Cu in galena, as occasionally reported, may therefore only occur when In or other trivalent ions are not present to facilitate coupled substitutions into sphalerite, or if sphalerite and other Cu sulphides are absent. Alternately, high Cu values in galena may be the result of substitution of Cu^{2+} directly for Pb^{2+}, however the Cu^{2+} ion would prefer sphalerite, and is generally rare; Cu^{+} is generally preferred in sulphide minerals (e.g., Goh et al., 2006). Only minor amounts of Ag^{+} can be expected in sphalerite due to its preferential incorporation into galena when present.

Since chalcopyrite is not a fully ionic structure, Goldschmidt's rules cannot be readily used to adequately predict partitioning patterns. Nevertheless, some inferences can be made from observed results and the partitioning of trace elements into sphalerite and galena. Compared to both sphalerite and galena, chalcopyrite is a relatively poor trace element carrier. Yet its ability to include trace elements is clearly increased at higher temperatures and/or pressures, where chalcopyrite can host high concentrations of Ga, In, Sn and sometimes Ag (authors as-yet

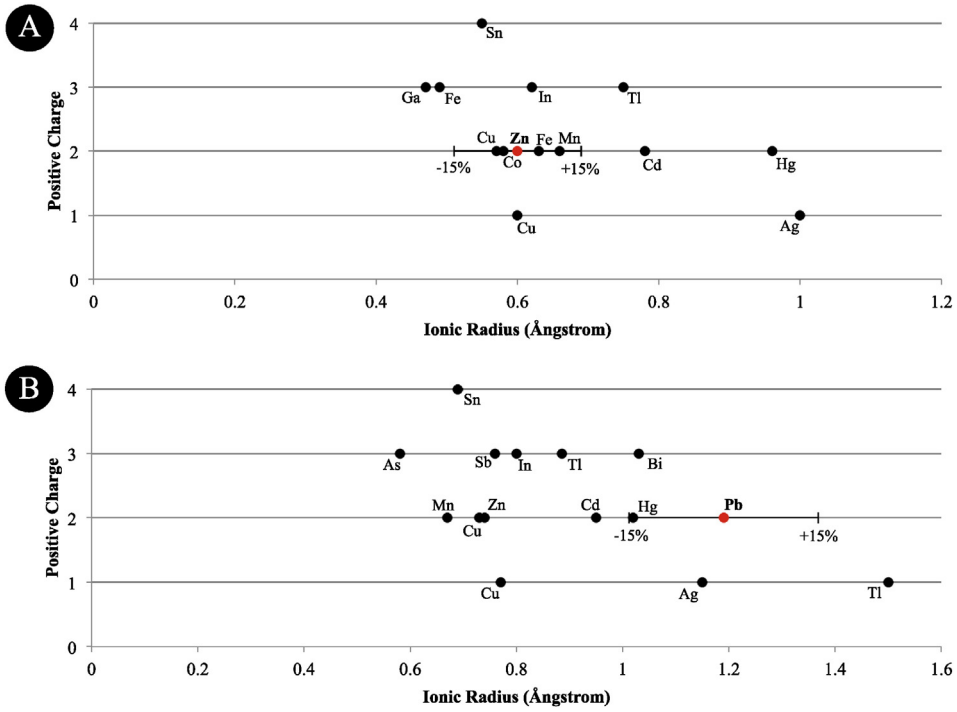

Fig. 9. Plots showing the ionic radius of various trace element ions in: (A) tetrahedral coordination (as in sphalerite) compared to Zn^{2+}; and (B) octahedral coordination (as in galena) compared to Pb^{2+} (data from Shannon, 1976).

unpublished data). Chalcopyrite may also become a more noteworthy trace element host in the absence of sphalerite and/or galena, or other carriers, notably chalcocite and bornite (e.g. chalcopyrite hosts significant Co and In in sample BB55, and Mn in sample Kmi2a in the absence of sphalerite). Despite this however, Harris et al. (1984) report analyses of high Ag-bearing chalcopyrite from two deposits (Izok Lake and Hilton), both of which contain galena.

6.3. Anomalies and exceptions

The authors are unaware of data for the ionic radius of Sn^{2+}, precluding prediction of the partitioning behaviour of this ion from Goldschmidt's rules. Indeed, Shannon (1976) states that it is impossible to define the ionic radius of Sn^{2+} since it varies depending on the degree of distortion of the host compound. In lower temperature (non-recrystallized) ores, sphalerite, galena and chalcopyrite are all primary Sn carriers in different samples. The partitioning behaviour of Sn below recrystallization conditions is thus likely to vary as a function of multiple parameters, whose relative influence differs from case to case. If Sn^{2+} is the typical cation hosted in these sulphides, then its erratic partitioning behaviour may be due to differences in sulphide crystal distortion.

The question remains why Hg is largely absent from galena, while sometimes present within co-crystallized sphalerite, considering that the Hg^{2+} ion falls within 15% of the Pb^{2+} ionic radius in octahedral coordination, while outside 15% of the Zn^{2+} ionic radius in tetrahedral coordination (Fig. 9A, B). Assuming both sphalerite and galena are present, preferential substitution of Hg^{2+} into sphalerite may be aided through direct solid solution with Hg-minerals. Metacinnabar (HgS), tiemannite (HgSe) and coloradoite (HgTe) are fully isostructural with sphalerite and complete solid solution has been reported between ZnS and HgS for example (Kremheller et al., 1960). Thus these minerals may contribute to the somewhat erratic partitioning behaviour of Hg across the sample suite, leading to its classification as a Group 3 trace element.

6.4. Implications

This study presents a tool that may be helpful in determining whether a given BMS assemblage co-crystallized. According to the factors considered here, if the BMS hosts of various trace elements in a given assemblage do not match the typical hosts described here (Table 4), it can then be suggested that the BMS did not co-crystallize. However, if the primary BMS hosts do match the typical hosts described here, then it may be suggestive of a co-crystallized assemblage. If both Ga and Sn, and possibly In, are primarily hosted in chalcopyrite in preference to either sphalerite or galena, then this may indicate that the BMS assemblage has recrystallized. Given the common association of sphalerite, galena and chalcopyrite in different ore types and geological environments (Bowles et al., 2011), the predictive understanding reached in this work has potentially wide application to a range of ore systems.

This tool may prove powerful in assessing co-crystallization of the BMS assemblage in systems with simple geological histories. However in systems that have more complex geological histories (i.e. where mobilization of trace elements occurs after BMS (re-)crystallization), it is conceivable for various trace elements to be hosted by a BMS mineral not normally preferred, even if those BMS co-crystallized. For example, in a limited number of LA-ICP-MS maps from Broken Hill, there is clear evidence that some Ag and Sb, as well as Co, has been leached out of galena and sphalerite respectively. The galena and sphalerite appear zoned as they are depleted in trace elements at grain boundaries and adjacent to fractures (Fig. 10; see also the Ag and Sb maps in Fig. 6). Growth zoning is exceptionally rare in recrystallized deposits due to high temperatures and ample time for grain-scale re-equilibration of trace elements. Thus the zoning in the Broken Hill samples is

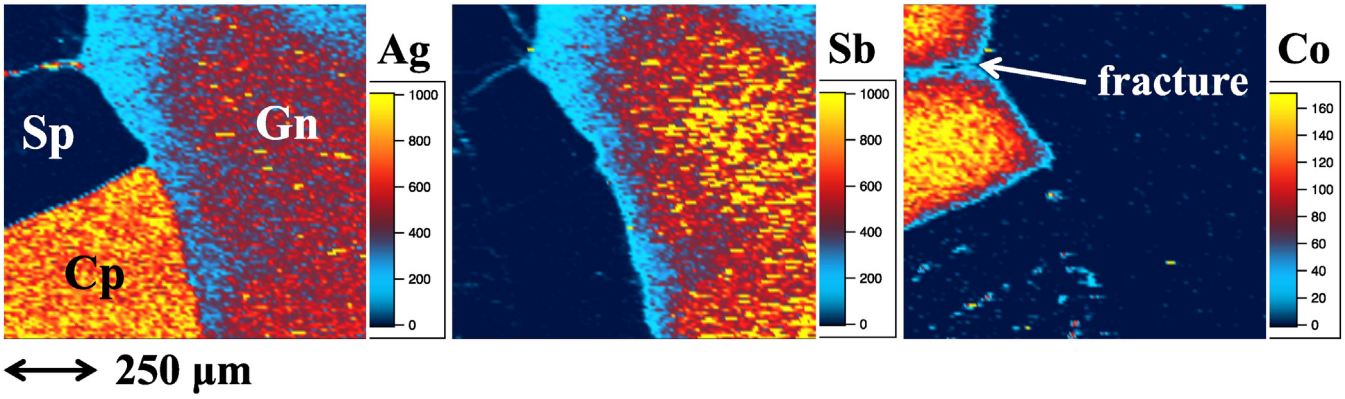

Fig. 10. LA-ICP-MS element maps (Ag, Sb, Co) of an assemblage comprising co-crystallized sphalerite (Sp), galena (Gn) and chalcopyrite (Cp) from the Broken Hill recrystallized SEDEX deposit (sample BH73). Note depletion of Ag and Sb in galena and Co in sphalerite at grain boundaries and adjacent to fracture. Concentration scales in parts-per-million (weight).

interpreted as the result of secondary sub-solidus leaching along grain boundaries and fractures as a result of fluid-rock interaction post re-crystallization. In the Broken Hill samples studied here, the apparent preferred sulphide host of Sb and Co is unchanged, whereas chalcopyrite now hosts more Ag than galena in sample BH73, contrary to what is normally preferred. It is thus apparent that such leaching, diffusion, or analogous sub-solidus processes, may markedly alter the trace element distribution patterns in a given BMS assemblage away from what is preferred during (re-) crystallization. Thus, a BMS assemblage that co-crystallized, but has since had trace elements mobilized and re-distributed within (or even outside) the assemblage, may now have a trace element distribution pattern that suggests the assemblage did not co-crystallize.

Although this work is principally concerned with the preferred BMS hosts for various trace elements rather than specific concentrations of trace elements within those sulphides, the data and interpretations provide an important foundation for future quantification of partitioning coefficients for trace elements in BMS pairs formed at equilibrium. Even if this work suggests that these ratios for many trace elements may not depend so heavily on external factors like temperature and pressure, it is nonetheless feasible that the partitioning of some trace elements between co-crystallizing BMS pairs has potential for quantitative geothermometry.

Various attempts have, in the past, been made to develop functional sulphide geothermometers utilizing trace element concentrations. Examples include using the chemical composition of Ag-rich tetrahedrite solid solutions (Sack, 2000, 2005; Gallego Hernández and Akasaka, 2010), or distributions of Cd and Mn between sphalerite/wurtzite and galena pairs to determine the temperature of ore formation (Bethke and Barton, 1971; Bortnikov et al., 1995). Analogous techniques have been established to calculate conditions of metamorphism using accessory minerals, for example using Ti in zircon or Zr in rutile or titanite (Watson et al., 2006; Ferry and Watson, 2007; Hayden et al., 2008) — methods that also have potential application in ore systems (Ismail et al., 2014).

Although encouraging results were obtained during the development of some trace element sulphide geothermometers, reliable calibration and routine application of such geothermometers was severely limited by the inability, at that time, to precisely quantify trace element concentrations at fine spatial resolutions *in-situ*. The site-specific sampling offered by modern microanalytical techniques opens the door for these approaches to be revitalized, and we would anticipate that useful BMS geothermometers will be developed in the future. Nevertheless, successful application of a geothermometer depends on analysing minerals that have co-crystallized at equilibrium. The identification of co-crystallized minerals can often be difficult and in many cases cannot be unequivocally confirmed and thus must be assumed from textural evidence; a critical problem in calibration of sulphide geothermometers, especially those based on natural samples. Trace element predictability as introduced here can be readily used for assessing co-crystallization of a BMS assemblage, and thus provides significant underpinning for future application of potential BMS geothermometers.

7. Conclusions

- The primary factors controlling the preferred BMS host for Mn, Fe, Co, Cu, Zn, Ga, As, Se, Ag, Cd, In, Sb, Te, Tl and Bi are element oxidation state, ionic radius of the substituting element, element availability and trace element budget of a given sulphide mineral.
- Temperature, pressure, redox conditions and metal source, do not appear to alter the preferred BMS host of Mn, Fe, Co, Cu, Zn, As, Se, Ag, Cd, Sb, Te, Hg, Tl and Bi.
- When sulphide recrystallization takes place at high metamorphic grades (amphibolite facies or above), the preferred BMS host for Ga and Sn usually becomes chalcopyrite. This is distinct from the favoured hosts in lower temperature regimes which, in the case of Ga, is sphalerite. During recrystallization, chalcopyrite may also become the preferred host for In, as distinct from sphalerite at lower temperatures.
- The partitioning behaviour of Sn below recrystallization conditions remains poorly constrained and shows little predictable pattern among the data presented here. Partitioning of Sn is likely to vary as a function of multiple parameters, the relative influence of which differs from case to case.
- Although general partitioning trends are identified for Co, Cu and Hg, these trends are not universally observed.
- Compared to sphalerite and galena, chalcopyrite is typically a poor trace element carrier, and generally only carries significant concentrations of trace elements in the absence of other BMS, or when formed at higher temperatures.
- Secondary leaching, diffusion, or analogous sub-solidus processes, may markedly alter the preferred trace element distribution patterns in a given sulphide assemblage post (re-) crystallization.

Acknowledgements

We are most grateful to the two reviewers, John Bowles and Louis Cabri, whose insight and expertise helped us to improve this manuscript. Laboratory assistance from Ben Wade and Aoife McFadden is also greatly appreciated.

Appendix A. Mean minimum detection limits (99% confidence). Data in ppm (molar).

Locality	Sample/sulfide	Element																
Herja	Hj13	Mn	Fe	Co	Cu	Zn	Ga	As	Se	Ag	Cd	In	Sn	Sb	Te	Hg	Tl	Bi
Romania	Sphalerite (10)	0.11	3.1	0.01	0.13	0.99	0.00	0.06	2.7	0.00	0.06	0.00	0.02	0.01	0.04	0.01	0.00	0.00
	Galena (10)	3.3	76	0.17	4.4	28	0.29	1.8	83	0.12	1.6	0.02	0.66	0.18	1.9	0.05	0.01	0.03
	Chalcopyrite (10)	0.06	1.6	0.00	0.12	0.47	0.00	0.03	1.8	0.00	0.03	0.00	0.01	0.00	–	0.00	0.00	0.00
Toroiaga	TOR191	Mn	Fe	Co	Cu	Zn	Ga	As	Se	Ag	Cd	In	Sn	Sb	Te	Hg	Tl	Bi
Romania	Sphalerite (10)	0.10	2.3	0.01	0.28	0.18	0.01	1.4	0.68	0.00	0.03	0.00	0.02	0.00	0.03	4.8	0.00	0.00
	Galena (10)	4.0	75	0.25	7.3	4.3	0.19	51	6.2	0.14	1.9	0.02	0.49	0.11	–	10	0.01	0.02
	Chalcopyrite (10)	0.07	1.6	0.00	0.27	0.09	0.00	0.84	0.49	0.00	0.02	0.00	0.01	0.00	0.03	4.3	0.00	0.00
	TOR197	Mn	Fe	Co	Cu	Zn	Ga	As	Se	Ag	Cd	In	Sn	Sb	Te	Hg	Tl	Bi
	Sphalerite (10)	0.09	2.0	0.01	0.26	0.18	0.01	1.1	0.71	0.00	0.05	0.00	0.02	0.00	0.03	7.1	0.00	0.00
	Galena (10)	6.2	114	0.43	13	7.5	0.34	–	384	0.16	2.1	0.04	0.91	0.22	0.73	6.5	0.02	0.03
	Chalcopyrite (10)	0.09	1.9	0.01	0.31	0.12	0.01	0.90	0.63	0.00	0.02	0.00	0.02	0.00	0.03	9.4	0.00	0.00
	Emeric2	Mn	Fe	Co	Cu	Zn	Ga	As	Se	Ag	Cd	In	Sn	Sb	Te	Hg	Tl	Bi
	Sphalerite (9)	0.13	3.3	–	0.19	1.8	0.01	0.07	3.5	0.00	0.12	0.00	0.03	0.01	–	0.01	0.00	0.00
	Galena (6)	2.5	63	0.15	4.0	26	0.22	1.5	–	–	1.7	0.02	0.55	0.19	–	0.04	0.01	0.02
	Chalcopyrite (9)	0.19	1.3	–	0.12	2.2	0.01	0.12	4.5	0.00	0.12	0.00	0.02	0.01	–	0.01	0.00	0.00
Baita Bihor	BBH16B	Mn	Fe	Co	Cu	Zn	Ga	As	Se	Ag	Cd	In	Sn	Sb	Te	Hg	Tl	Bi
Romania	Sphalerite (10)	0.09	2.3	0.01	0.14	1.7	0.01	0.05	2.8	0.00	0.09	0.00	0.02	0.01	0.06	0.01	0.00	0.00
	Galena (10)	5.6	136	0.33	7.3	62	0.36	2.0	65	0.16	2.6	0.04	0.72	0.23	–	0.01	0.02	0.04
	BBH20	Mn	Fe	Co	Cu	Zn	Ga	As	Se	Ag	Cd	In	Sn	Sb	Te	Hg	Tl	Bi
	Sphalerite (10)	0.09	2.4	0.01	0.13	1.6	0.01	0.05	2.3	0.00	0.10	0.00	0.02	0.01	0.06	0.01	0.00	0.00
	Galena (10)	3.9	103	0.28	5.2	51	0.21	2.0	102	0.14	2.7	0.03	0.93	0.29	–	0.06	0.02	0.06
	BB55	Mn	Fe	Co	Cu	Zn	Ga	As	Se	Ag	Cd	In	Sn	Sb	Te	Hg	Tl	Bi
	Galena (10)	7.3	178	0.52	11	65	0.37	2.4	82	0.20	2.2	0.06	1.1	0.35	–	0.02	0.02	0.06
	Chalcopyrite (10)	0.06	1.3	0.00	0.13	0.58	0.01	0.04	1.8	0.00	0.04	0.00	0.01	0.00	0.03	0.00	0.00	0.00
	BBH32	Mn	Fe	Co	Cu	Zn	Ga	As	Se	Ag	Cd	In	Sn	Sb	Te	Hg	Tl	Bi
	Sphalerite (10)	0.06	2.3	0.02	0.24	0.13	0.00	0.57	0.43	0.00	0.01	0.00	0.01	0.00	0.02	2.0	0.00	0.00
	Galena (10)	1.8	40	0.11	7.1	3.0	0.13	16	12	0.08	0.68	0.02	0.41	0.20	0.72	18	0.01	0.05
Oravita	ORV4B	Mn	Fe	Co	Cu	Zn	Ga	As	Se	Ag	Cd	In	Sn	Sb	Te	Hg	Tl	Bi
Romania	Sphalerite (10)	0.07	1.4	0.00	0.18	0.16	0.01	0.48	0.45	0.00	0.02	0.00	0.01	0.00	0.02	3.5	0.00	0.00
	Galena (10)	1.2	26	0.07	3.3	1.8	0.07	11	8.1	0.05	0.41	0.01	0.24	0.06	0.33	52	0.01	0.01
	Chalcopyrite (10)	0.08	1.5	0.00	0.28	0.13	0.00	0.52	0.51	0.00	0.02	0.00	0.02	0.00	0.02	5.3	0.00	0.00
Kapp Mineral	Kmi2a	Mn	Fe	Co	Cu	Zn	Ga	As	Se	Ag	Cd	In	Sn	Sb	Te	Hg	Tl	Bi
Norway	Galena (10)	3.9	58	0.35	10	6.9	0.19	12	15	0.10	2.7	0.03	0.50	0.08	–	5.5	0.01	0.02
	Chalcopyrite (10)	0.09	31	0.01	10	0.32	0.01	0.96	0.70	0.10	0.07	0.00	0.03	0.02	0.04	10	0.00	0.00
	Kmi5	Mn	Fe	Co	Cu	Zn	Ga	As	Se	Ag	Cd	In	Sn	Sb	Te	Hg	Tl	Bi
	Sphalerite (10)	0.10	2.1	0.01	0.17	1.8	0.01	0.08	3.3	0.00	0.07	0.00	0.02	0.01	0.05	0.01	0.00	0.00
	Galena (10)	6.6	131	0.48	7.9	60	0.27	2.6	15	0.15	1.4	0.03	0.64	0.31	–	0.01	0.01	0.04
Mt. Isa	5985C1	Mn	Fe	Co	Cu	Zn	Ga	As	Se	Ag	Cd	In	Sn	Sb	Te	Hg	Tl	Bi
Australia	Sphalerite (5)	0.11	3.3	0.01	0.29	0.17	0.01	1.5	0.88	0.00	0.03	0.00	0.03	0.01	0.03	4.6	0.00	0.00
	Galena (4)	5.2	87	0.35	8.0	6.3	0.23	2804	9.2	0.11	1.5	0.03	0.76	0.17	0.71	9.3	0.01	0.03
Bleikvassli	Bv-1	Mn	Fe	Co	Cu	Zn	Ga	As	Se	Ag	Cd	In	Sn	Sb	Te	Hg	Tl	Bi
Norway	Sphalerite (10)	0.09	2.0	0.01	0.12	0.96	0.01	0.11	1.7	0.00	0.06	0.00	0.03	0.01	0.05	0.01	0.00	0.00
	Galena (10)	3.9	80	–	5.4	35	–	3.2	1902	0.14	2.3	0.04	0.90	0.35	–	0.07	0.01	0.06
	Chalcopyrite (5)	0.06	1.2	0.00	0.09	0.52	0.00	0.06	1.0	0.00	0.03	0.00	0.02	0.01	0.03	0.00	0.00	0.00
	V598572	Mn	Fe	Co	Cu	Zn	Ga	As	Se	Ag	Cd	In	Sn	Sb	Te	Hg	Tl	Bi
	Sphalerite (5)	0.13	3.3	0.01	0.22	1.3	0.01	0.24	4.5	0.01	0.07	0.00	0.03	0.01	–	0.01	0.00	0.00
	Galena (10)	2.9	67	0.26	4.1	23	0.15	4.7	52	0.12	1.4	0.03	0.59	0.20	–	0.04	0.01	0.04
	Chalcopyrite (9)	0.06	1.6	0.00	0.14	0.55	0.00	0.09	1.8	0.00	0.03	0.00	0.02	0.01	0.02	0.00	0.00	0.00
Broken Hill	BH73	Mn	Fe	Co	Cu	Zn	Ga	As	Se	Ag	Cd	In	Sn	Sb	Te	Hg	Tl	Bi
Australia	Sphalerite (10)	0.12	3.7	0.01	0.16	1.1	0.01	0.07	2.3	0.00	0.06	0.00	0.03	0.01	0.05	0.01	0.00	0.00
	Galena (10)	3.1	90	0.13	4.2	26	0.15	1.9	34	0.09	1.1	0.03	0.81	0.29	1.2	0.05	0.02	0.07
	Chalcopyrite (5)	0.17	5.3	0.01	0.29	1.5	0.01	0.10	3.2	0.01	0.09	0.00	0.05	0.02	0.10	0.02	0.00	0.00
	BH218	Mn	Fe	Co	Cu	Zn	Ga	As	Se	Ag	Cd	In	Sn	Sb	Te	Hg	Tl	Bi
	Sphalerite (10)	0.10	2.5	0.01	0.14	1.5	0.01	0.07	3.2	0.00	0.09	0.00	0.02	0.01	–	0.01	0.00	0.00
	Galena (10)	3.4	75	0.27	3.9	38	0.24	2.5	162	0.10	2.4	0.02	0.74	0.18	–	0.05	0.01	0.04
Mofjellet	Mo2	Mn	Fe	Co	Cu	Zn	Ga	As	Se	Ag	Cd	In	Sn	Sb	Te	Hg	Tl	Bi
Norway	Sphalerite (10)	0.05	1.1	0.01	0.21	0.16	0.00	0.47	0.39	0.00	0.01	0.00	0.01	0.00	0.02	2.4	0.00	0.00
	Galena (10)	3.2	66	0.24	12	6.5	0.27	31	17	0.15	1.3	0.02	0.61	0.22	0.96	363	0.01	0.05

References

Bajwah, Z., Seccombe, P., Offler, R., 1987. Trace element distribution, Co: Ni ratios and genesis of the Big Cadia iron-copper deposit, New South Wales, Australia. Mineral. Deposita 22, 292–300.

Becker, W., Lutz, H., 1978. Phase studies in the systems CoS–MnS, CoS–ZnS, and CoS–CdS. Mater. Res. Bull. 13, 907–911.

Bethke, P.M., Barton, P.B., 1971. Distribution of some minor elements between coexisting sulphide minerals. Econ. Geol. 66, 140–163.

Bjerkgård, T., Marker, M., Sandstad, J., Cook, N., Sørdahl, T., 2001. Ore potential with emphasis on gold in the Mofjellet deposit, Rana, Nordland, Norway. NGU report.

Blackburn, W.H., Schwendeman, J.F., 1977. Trace-element substitution in galena. Can. Mineral. 15, 365–373.

Borcos, M., Lang, B., Bostinescu, S., Gheorghita, I., 1975. Neogene hydrothermal ore deposits in the volcanic Gutai Mountains, part III. Revue Roumaine de Geologie, Geophysique et Geographie, Serie de Geologie 19, pp. 21–35.

Bortnikov, N., Dobrovol'skaya, M., Genkin, A., Naumov, V., Shapenko, V., 1995. Sphalerite–galena geothermometers; distribution of cadmium, manganese, and the fractionation of sulfur isotopes. Econ. Geol. 90, 155–180.

Bortnikov, N.S., Cabri, L.J., Vikent'ev, I.V., McMahon, G., Bogdanov, Y.A., 2000. Invisible gold in sulfides from recent submarine hydrothermal vents. Dokl. Earth Sci. 373, 863–866.

Bowles, J.F.W., Howie, R.A., Vaughan, D.J., Zussman, J., 2011. Rock-forming Minerals: non-silicates: oxides, hydroxides and sulphides. Geol. Soc. Lond.

Brill, B., 1989. Trace-element contents and partitioning of elements in ore minerals from the CSA Cu–Pb–Zn deposit, Australia. Can. Mineral. 27, 263–274.

Bryndzia, L.T., Scott, S.D., Spry, P.G., 1990. Sphalerite and hexagonal pyrrhotite geobarometer; correction in calibration and application. Econ. Geol. 85, 408–411.

Cabri, L.J., 1992. The distribution of trace precious metals in minerals and mineral products. The 23rd Hallimond Lecture. Mineral. Mag. 56, 298–308.

Cabri, L.J., Campbell, J.L., Laflamme, J.G., Leigh, R.G., Maxwell, J.A., Scott, J.D., 1985. Proton-microprobe analysis of trace elements in sulphides from some massive-sulphide deposits. Can. Mineral. 23, 133–148.

Cabri, L.J., McMahon, G., Bortnikov, N.S., Vikentiev, I.V., Bogdanov, Y.A., 2000. SIMS gold analyses of sea floor sulfide minerals. In: Benninghoven, A., Bertrand, P., Migeon, H.-N., Werner, H.W. (Eds.), SIMS XII, Proceedings, 12th International Conference on Secondary Ion Mass Spectrometry, Brussels, Belgium. Elsevier, pp. 1019–1022.

Chen, W.W., Zhang, J.M., Ardell, A.J., Dunn, B., 1988. Solid-state phase equilibria in the ZnS–CdS system. Mater. Res. Bull. 23, 1667–1673.

Chutas, N.I., Kress, V.C., Ghiorso, M.S., Sack, R.O., 2008. A solution model for high-temperature PbS–$AgSbS_2$–$AgBiS_2$ galena. Am. Mineral. 93, 1630–1640.

Ciobanu, C.L., Cook, N.J., Stein, H., 2002. Regional setting and geochronology of the Late Cretaceous banatitic magmatic and metallogenetic belt. Mineral. Deposita 37, 541–567.

Ciobanu, C.L., Cook, N.J., Kelson, C.R., Guerin, R., Kalleske, N., Danyushevsky, L., 2013. Trace element heterogeneity in molybdenite fingerprints stages of mineralization. Chem. Geol. 347, 175–189.

Ciobanu, C.L., Brugger, J., Cook, N.J., Mills, S.J., Elliott, P., Damian, G., Damian, F., 2014. Graţianite, $MnBi_2S_4$, a new mineral from the Băiţa Bihor skarn, Romania. Am. Mineral. 99, 1163–1170.

Cioflica, G., Vlad, S., 1981. Cupriferous mineralization at Ciclova. An Univ Bucuresti Ser Geol 30, 1–17.

Cioflica, G., Vlad, S., Stoici, S., 1971. Repartition de la mineralisation dans les skarns de Baita Bihorului. Revue Roumaine de Geologie, Geophysique et Geographie, Serie de Geologie 15, pp. 43–58.

Cioflica, G., Vlad, S., Volanschi, E., Stoici, S., 1977. Magnesian skarns and associated mineralization at Baita Bihor. St. Cerc. Geol. Geofiz. Geogr. Ser. Geol 22, 39–57.

Cioflica, G., Jude, R., Lupulescu, M., Simon, G., Damian, G., 1995. New data on the Bi-minerals from the mineralizations related to Paleocene magmatites in Romania. Romanian J. Mineral. 76, 9–23.

Cioflica, G., Lupulescu, M., Shimizu, M., 1997. Bismuth minerals from the Baita Bihor and Valisor–Tincova mines: new compositional data. Romanian J. Mineral. 78, 13–14.

Constantinescu, E., Ilinca, G., Ilinca, A., 1988. Laramian hydrothermal alteration and ore deposition in the Oravita-Ciclova area. Southwestern Banat. DS Inst Geol Geofiz 72-73, 13–26.

Cook, N.J., 1993. Conditions of metamorphism estimated from alteration lithologies and ore at the Bleikvassli Zn–Pb–(Cu) deposit, Nordland, Norway. Nor. Geol. Tidsskr. 73, 226–233.

Cook, N.J., 1997. Bismuth and bismuth-antimony sulphosalts from Neogene vein mineralisation, Baia Borsa area, Maramures, Romania. Mineral. Mag. 61, 387–409.

Cook, N.J., 2001. Ore mineralogical investigation of the Mofjell deposit (Mo i Rana, Nordland, Norway) with emphasis on gold and silver distribution. Norges Geologiske Undersokelse Report.

Cook, N.J., Ciobanu, C.L., 2003. Cervelleite, Ag_4TeS, from three localities in Romania, substitution of Cu, and the occurrence of the associated phase, Ag_2Cu_2TeS. Neues Jahrb. Mineral. Monatshefte 321–336.

Cook, N.J., Damian, G.S., 1997. New data on "plumosite" and other sulphosalt minerals from the Herja hydrothermal vein deposit, Baia Mare district, Rumania. Geol. Carpath. 48, 387–399.

Cook, N.J., Spry, P.G., Vokes, F.M., 1998. Mineralogy and textural relationships among sulphosalts and related minerals in the Bleikvassli Zn–Pb–(Cu) deposit, Nordland, Norway. Mineral. Deposita 34, 35–56.

Cook, N.J., Ciobanu, C.L., Pring, A., Skinner, W., Shimizu, M., Danyushevsky, L., Saini-Eidukat, B., Melcher, F., 2009. Trace and minor elements in sphalerite: A LA-ICPMS study. Geochim. Cosmochim. Acta 73, 4761–4791.

Cook, N.J., Ciobanu, C.L., Danyushevsky, L.V., Gilbert, S., 2011a. Minor and trace elements in bornite and associated Cu–(Fe)-sulphides: A LA-ICP-MS study. Geochim. Cosmochim. Acta 75, 6473–6496.

Cook, N.J., Sundblad, K., Valkama, M., Nygård, R., Ciobanu, C.L., Danyushevsky, L., 2011b. Indium mineralisation in A-type granites in southeastern Finland: insights into mineralogy and partitioning between coexisting minerals. Chem. Geol. 284, 62–73.

Cook, N.J., Ciobanu, C.L., Brugger, J., Etschmann, B., Howard, D.L., de Jonge, M.D., Ryan, C., Paterson, D., 2012. Determination of the oxidation state of Cu in substituted Cu–In–Fe-bearing sphalerite via μ-XANES spectroscopy. Am. Mineral. 97, 476–479.

Cook, N.J., Etschmann, B., Ciobanu, C.L., Geraki, K., Howard, D., Williams, T., Rae, N., Pring, A., Chen, G., Johannessen, B., Brugger, J., 2015. Distribution and Substitution Mechanism of Ge in a Ge–(Fe)-Bearing Sphalerite. Minerals 5, 117–132.

Craig, J.R., Kullerud, G., 1968. Phase relations and mineral assemblages in the copper-lead-sulfur system. Am. Mineral. 53, 145–161.

Dare, S.A., Barnes, S.-J., Prichard, H.M., Fisher, P.C., 2011. Chalcophile and platinum-group element (PGE) concentrations in the sulfide minerals from the McCreedy East deposit, Sudbury, Canada, and the origin of PGE in pyrite. Mineral. Deposita 46, 381–407.

Emslie, D., Beukes, G., 1981. Minor-and trace-element distribution in sphalerite and galena from the Otavi Mountainland, South West Africa. Ann. Geol. Surv. Republic of South Africa 15, 11–28.

Ferry, J., Watson, E., 2007. New thermodynamic models and revised calibrations for the Ti-in-zircon and Zr-in-rutile thermometers. Contrib. Mineral. Petrol. 154, 429–437.

Flood, B., 1967. Sulphide mineralizations within the Hecla Hoek complex in Vestspitsbergen and Bjørnøya. Norsk Polarinstitutt Årbok, pp. 109–127.

Foord, E.E., Shawe, D.R., 1989. The Pb–Bi–Ag–Cu–(Hg) chemistry of galena and some associated sulfosalts: a review and some new data from Colorado, California and Pennsylvania. Can. Mineral. 27, 363–382.

Frost, B.R., Mavrogenes, J.A., Tomkins, A.G., 2002. Partial melting of sulphide ore deposits during medium-and high-grade metamorphism. Can. Mineral. 40, 1–18.

Frost, B.R., Swapp, S.M., Gregory, R.W., 2005. Prolonged existence of sulphide melt in the Broken Hill orebody, New South Wales, Australia. Can. Mineral. 43, 479–493.

Gallego Hernández, A.N., Akasaka, M., 2010. Ag-rich Tetrahedrite in the El Zancudo Deposit, Colombia: Occurrence, Chemical Compositions and Genetic Temperatures. Resour. Geol. 60, 218–233.

George, L., Cook, N.J., Ciobanu, C.L., Wade, B., 2015. Trace and minor elements in galena: A reconnaissance LA-ICP-MS study. Am. Mineral. 100, 548–569.

Gheorghitescu, D., 1975. Mineralogical and geochemical study of formations in the thermal, metasomatic contact at Oravita (Cosovita). DS Inst Geol Geofiz 61, 59–103.

Goh, S.W., Buckley, A.N., Lamb, R.N., Rosenberg, R.A., Moran, D., 2006. The oxidation states of copper and iron in mineral sulphides, and the oxides formed on initial exposure of chalcopyrite and bornite to air. Geochim. Cosmochim. Acta 70, 2210–2228.

Goldschmidt, V.M., 1954. Geochemistry. Soil Sci. 78, 156.

Gotz, A., Damian, G., Farbas, N., 1990. Contributii la mineralogia bournonitul associat mineralizatiilor din masivul Toroiaga-Baia Borsa. Rev. Mineral. 41, 467–471.

Hall, S.R., Stewart, J.M., 1973. The crystal structure refinement of chalcopyrite, $CuFeS_2$. Acta Crystallogr. 29, 579–585.

Hannan, K.W., Golding, S.D., Herbert, H.K., Krouse, H.R., 1993. Contrasting alteration assemblages in metabasites from Mount Isa, Queensland; implications for copper ore genesis. Econ. Geol. 88, 1135–1175.

Harris, D.C., Cabri, L.J., Nobiling, R., 1984. Silver-bearing chalcopyrite, a principal source of silver in the Izok Lake massive-sulphide deposit; confirmation by electron- and proton-microprobe analyses. Can. Mineral. 22, 493–498.

Hayden, L.A., Watson, E.B., Wark, D.A., 2008. A thermobarometer for sphene (titanite). Contrib. Mineral. Petrol. 155, 529–540.

Haydon, R.C., McConachy, G.W., 1987. The stratigraphic setting of Pb–Zn–Ag mineralization at Broken Hill. Econ. Geol. 82, 826–856.

Holwell, D., McDonald, I., 2010. A review of the behaviour of platinum group elements within natural magmatic sulphide ore systems. Platin. Met. Rev. 54, 26–36.

Huston, D.L., Sie, S.H., Suter, G.F., Cooke, D.R., Both, R.A., 1995. Trace elements in sulphide minerals from eastern Australian volcanic-hosted massive sulphide deposits; Part I, Proton microprobe analyses of pyrite, chalcopyrite, and sphalerite, and Part II, Selenium levels in pyrite; comparison with delta 34 S values and implications for the source of sulfur in volcanogenic hydrothermal systems. Econ. Geol. 90, 1167–1196.

Ilinca, G., Makovicky, E., Topa, D., Zagler, G., 2012. Cuproneyite, $Cu_7Pb_{27}Bi_{25}S_{68}$, a new mineral species from Baita Bihor, Romania. Can. Mineral. 50, 353–370.

Ismail, R., Ciobanu, C.L., Cook, N.J., Teale, G.S., Giles, D., Schmidt Mumm, A., Wade, B., 2014. Rare earths and other trace elements in minerals from skarn assemblages, Hillside iron oxide–copper–gold deposit, Yorke Peninsula, South Australia. Lithos 184, 456–477.

Johan, Z., 1988. Indium and germanium in the structure of sphalerite: an example of coupled substitution with copper. Mineral. Petrol. 39, 211–229.

Katona, I., Pascal, M.-L., Fonteilles, M., Verkaeren, J., 2003. The melilite (Gh_{50}) skarns of Oraviţa, Banat, Romania: transition to gehlenite (Gh_{85}) and to vesuvianite. Can. Mineral. 41, 1255–1270.

Kojima, S., Sugaki, A., 1984. Phase relations in the central portion of the Cu–Fe–Zn–S system between 800° and 500 °C. Mineral. J. 12, 15–28.

Kojima, S., Sugaki, A., 1985. Phase relations in the Cu–Fe–Zn–S system between 500 degrees and 300 degrees C under hydrothermal conditions. Econ. Geol. 80, 158–171.

Krämer, V., Hirth, H., Hofherr, M., Trah, H.-P., 1987. Phase studies in the systems Ag_2Te–Ga_2Te_3, ZnSe–In_2Se_3 and ZnS–Ga_2S_3. Thermochim. Acta 112, 88–94.

Kremheller, A., Levine, A.K., Gashurov, G., 1960. Hydrothermal preparation of two-component solid solutions from II–VI compounds. J. Electrochem. Soc. 107, 12–15.

Lang, B., 1979. The base metals-gold hydrothermal ore deposits of Baia Mare, Romania. Econ. Geol. 74, 1336–1351.

Large, R.R., Bull, S.W., McGoldrick, P.J., Derrick, G., Carr, G., Walters, S., 2005. Stratiform and strata-bound Zn–Pb–Ag + Cu deposits of the Proterozoic sedimentary basins of northern Australia. Economic Geology 100th Anniversary Volume, pp. 931–963.

Larocque, A.C.L., Jackman, J.A., Cabri, L.J., Hodgson, C.J., 1995. Calibration and analysis of Ag in pyrite and chalcopyrite by Secondary Ion Mass Spectrometry (SIMS) and preliminary results from the Mobrun VMS deposit, Rouyn-Noranda, Quebec. Can. Mineral. 33, 361–372.

Lepetit, P., Bente, K., Doering, T., Luckhaus, S., 2003. Crystal chemistry of Fe-containing sphalerites. Phys. Chem. Miner. 30, 185–191.

Leyh, W.R., Conor, C.H., 2000. Stratigraphically controlled metallogenic zonation associated with the regional redox boundary of the Willyama Supergroup—economic implications for the southern Curnamona Province. Mesa J. 16, 39–47.

Liu, H., Chang, L.L.Y., 1994. Phase relations in the system PbS–PbSe–PbTe. Mineral. Mag. 58, 567–578.

Lockington, J., Cook, N.J., Ciobanu, C.L., 2014. Trace and minor elements in sphalerite from metamorphosed sulphide deposits. Mineral. Petrol. 108, 873–890.

Lottermoser, B., 1989. Rare earth element study of exhalites within the Willyama Supergroup, Broken Hill Block, Australia. Mineral. Deposita 24, 92–99.

Marincea, Ş., Dumitraş, D.-G., Ghineţ, C., Fransolet, A.-M., Hatert, F., Rondeaux, M., 2011. Gehlenite from three occurrences of high-temperature skarns, Romania: new mineralogical data. Can. Mineral. 49, 1001–1014.

Mathias, B., Clark, G., 1975. Mount Isa copper and silver-lead-zinc orebodies—Isa and Hilton mines. Econ. Geol. Australia Papua New Guinea 1, 351–372.

Mavrogenes, J., MacIntosh, I., Ellis, D., 2001. Partial melting of the Broken Hill galena–sphalerite ore: experimental studies in the system PbS–FeS–ZnS–(Ag_2S). Econ. Geol. 96, 205–210.

McIntyre, N.S., Cabri, L.J., Chauvin, W.J., Laflamme, J.H.G., 1984. Secondary ion mass spectrometric study of dissolved silver and indium in sulfide minerals. Scan. Electron Microsc. 3, 1139–1146.
Mikhlin, Y., Tomashevich, Y., Tauson, V., Vyalikh, D., Molodtsov, S., Szargan, R., 2005. A comparative X-ray absorption near-edge structure study of bornite, Cu_5FeS_4, and chalcopyrite, $CuFeS_2$. J. Electron Spectrosc. Relat. Phenom. 142, 83–88.
Moggi-Cecchi, V., Cipriani, C., Rossi, P., Ceccato, D., Rudello, V., Somacal, H., 2002. Trace element contents and distribution maps of chalcopyrite: a micro-PIXE study. Periodico di Mineralogia 71, 101–109.
Müller, W., Shelley, M., Miller, P., Broude, S., 2009. Initial performance metrics of a new custom-designed ArF excimer LA-ICPMS system coupled to a two-volume laser-ablation cell. J. Anal. At. Spectrom. 24, 209–214.
Neubauer, F., Lips, A., Kouzmanov, K., Lexa, J., Ivascanu, P., 2005. Subduction, slab detachment and mineralization: the Neogene in the Apuseni Mountains and Carpathians. Ore Geol. Rev. 27, 13–44.
Painter, M.G., Golding, S.D., Hannan, K.W., Neudert, M.K., 1999. Sedimentologic, petrographic, and sulfur isotope constraints on fine-grained pyrite formation at Mount Isa Mine and environs, Northwest Queensland, Australia. Econ. Geol. 94, 883–912.
Parr, J., Plimer, I., 1993. Models for Broken Hill-type lead-zinc-silver deposits: mineral deposit modeling. Geol. Assoc. Can. Spec. Pap. 40, 253–288.
Pearce, C.I., Pattrick, R.A.D., Vaughan, D.J., Henderson, C.M.B., Van der Laan, G., 2006. Copper oxidation state in chalcopyrite: Mixed Cu d^9 d^{10} characteristics. Geochim. Cosmochim. Acta 70, 4635–4642.
Perkins, W., 1997. Mount Isa lead-zinc orebodies: replacement lodes in a zoned syndeformational copper-lead-zinc system? Ore Geol. Rev. 12, 61–110.
Phillips, G.N., 1981. Water activity changes across an amphibolite-granulite facies transition, Broken Hill, Australia. Contrib. Mineral. Petrol. 75, 377–386.
Philpotts, J.A., 1978. The law of constant rejection. Geochim. Cosmochim. Acta 42, 909–920.
Plimer, I., 2007. The world's largest Zn–Pb–Ag deposit: a re-evaluation of Broken Hill (Australia). Mineral deposits: digging deeper. Irish Association for Economic Geology, Dublin, pp. 1239–1242.
Qian, Z., 1987. Trace elements in galena and sphalerite and their geochemical significance in distinguishing the genetic types of Pb–Zn ore deposits. Chin. J. Geochem. 6, 177–190.
Renock, D., Becker, U., 2011. A first principles study of coupled substitution in galena. Ore Geol. Rev. 42, 71–83.
Ringwood, A., 1955. The principles governing trace element distribution during magmatic crystallization Part I: the influence of electronegativity. Geochim. Cosmochim. Acta 7, 189–202.
Rosenberg, J., Spry, P., Jacobson, C., Cook, N., Vokes, F., 1998. Thermobarometry of the Bleikvassli Zn–Pb–(Cu) deposit, Nordland, Norway. Mineral. Deposita 34, 19–34.
Rosenberg, J., Spry, P., Jacobson, C., Vokes, F., 2000. The effects of sulfidation and oxidation during metamorphism on compositionally varied rocks adjacent to the Bleikvassli Zn–Pb–(Cu) deposit, Nordland, Norway. Mineral. Deposita 35, 714–726.
Rubenach, M.J., 1992. Proterozoic low-pressure/high-temperature metamorphism and an anticlockwise P–T–t path for the Hazeldene area, Mount Isa Inlier, Queensland, Australia. J. Metamorph. Geol. 10, 333–346.
Saager, R., 1967. Drei Typen von Kieslagerstätten im Mofjell-Gebiet, Nordland und ein neuer Vorschlag zur Gliederung der Kaledonischen Kieslager Norwegens. Nor. Geol. Tidsskr. 8, 68–73.
Sack, R.O., 2000. Internally consistent database for sulphides and sulfosalts in the system Ag_2S–Cu_2S–ZnS–Sb_2S_3–As_2S_3. Geochim. Cosmochim. Acta 64, 3803–3812.
Sack, R.O., 2005. Internally consistent database for sulphides and sulfosalts in the system Ag_2S-Cu_2S-ZnS-FeS-Sb_2S_3-As_2S_3: update. Geochim. Cosmochim. Acta 69, 1157–1164.
Shannon, R., 1976. Revised effective ionic radii and systematic studies of interatomic distances in halides and chalcogenides. Acta Crystallogr. Sect. A: Cryst. Phys., Diffr., Theor. Gen. Crystallogr. 32, 751–767.
Shimizu, M., Cioflica, G., Lupulescu, M., 1995. Ore mineralogy of Romanian deposits. Part I. Stanija and Baita Bihor, Apuseni Mountains and Tincova-Valisor, Banat (SW Carpathians), Romania. Japanese Mag. Mineral. Petrol. Sci. 45, 280–281.
Sombuthawee, C., Bonsall, S., Hummel, F., 1978. Phase equilibria in the systems ZnS–MnS, ZnS–$CuInS_2$, and MnS–$CuInS_2$. J. Solid State Chem. 25, 391–399.
Spry, P.G., Plimer, I.R., Teale, G.S., 2008. Did the giant Broken Hill (Australia) Zn–Pb–Ag deposit melt? Ore Geol. Rev. 34, 223–241.
Szöke, A., Steclaci, L., 1962. Regiunea Toroiaga, Baia-Borsa: studiu geologic, petrografic, mineralogic sï geochimic. Editura Academiei Republicii Populare Romine.
Todd, E.C., Sherman, D.M., 2003. Surface oxidation of chalcocite (Cu_2S) under aqueous (pH = 2–11) and ambient atmospheric conditions: mineralogy from Cu L-and O K-edge X-ray absorption spectroscopy. Am. Mineral. 88, 1652–1656.
Todd, E., Sherman, D., Purton, J., 2003. Surface oxidation of chalcopyrite ($CuFeS_2$) under ambient atmospheric and aqueous (pH 2–10) conditions: Cu, Fe L-and O K-edge X-ray spectroscopy. Geochim. Cosmochim. Acta 67, 2137–2146.
Van Achterbergh, E., Ryan, C., Jackson, S., Griffin, W., 2001. Data reduction software for LA-ICP-MS: Laser-Ablation-ICPMS in the earth sciences—principles and applications. Minerealogical Association of Canada (short course series) 29, pp. 239–243.
Vokes, F.M., 1963. Geological studies on the Caledonian Pyritic Zinc-Lead Orebody at Bleikvassli, Norland. Universitetsforlaget, Norway.
Vokes, F.M., 1966. On the possible modes of origin of the Caledonian sulphide ore deposit at Bleikvassli, Nordland, Norway. Econ. Geol. 61, 1130–1139.
von Cotta, B., 1864. Erzlagerstätten im Banat und in Serbien. Braumüller.
Watson, E., Wark, D., Thomas, J., 2006. Crystallization thermometers for zircon and rutile. Contrib. Mineral. Petrol. 151, 413–433.
Wilson, S., Ridley, W., Koenig, A., 2002. Development of sulphide calibration standards for the laser ablation inductively-coupled plasma mass spectrometry technique. J. Anal. At. Spectrom. 17, 406–409.
Ye, L., Cook, N.J., Ciobanu, C.L., Yuping, L., Qian, Z., Tiegeng, L., Wei, G., Yulong, Y., Danyushevskiy, L., 2011. Trace and minor elements in sphalerite from base metal deposits in South China: a LA-ICPMS study. Ore Geol. Rev. 39, 188–217.